



LUND
UNIVERSITY



STRENGTH AND STIFFNESS OF CROSS LAMINATED TIMBER AT IN-PLANE BEAM LOADING

HENRIK DANIELSSON, MARIO JELEC
and ERIK SERRANO

Structural
Mechanics

DEPARTMENT OF CONSTRUCTION SCIENCES
DIVISION OF STRUCTURAL MECHANICS
ISRN LUTVDG/TVSM--17/7164--SE (1-65) | ISSN 0281-6679

STRENGTH AND STIFFNESS OF CROSS LAMINATED TIMBER AT IN-PLANE BEAM LOADING

HENRIK DANIELSSON, MARIO JELEC
and ERIK SERRANO

Copyright © 2017 Division of Structural Mechanics,
Faculty of Engineering LTH, Lund University, Sweden.

For information, address:
Div. of Structural Mechanics,
Faculty of Engineering LTH, Lund University, Box 118, SE-221 00 Lund, Sweden.
Homepage: www.byggmek.lth.se

ABSTRACT

This report concerns element strength and stiffness of cross laminated timber (CLT) at in-plane beam loading and includes presentation of experimental investigations and a review of some analytical models for structural analysis. A total of 20 individual tests were carried out, divided into five different test series which each comprise four nominally equal tests. The test series include prismatic beams (two test series), beams with a hole (two test series) and beams with an end-notch (one test series). All CLT elements were composed of 5 layers of laminations, with three layers of longitudinal laminations of width 40 mm and two layers of transversal laminations of width 20 mm.

Test results relating to beam strength are presented in terms of maximum applied load and also in terms of stress components as calculated by analytical models. The review of models for stress analysis reveals significant influence of the element layup and laminations width on the predicted stresses. Test results relating to beam stiffness are present as element shear stiffness and element local and global modulus of elasticity, evaluated based on the European test standard EN 408.

Keywords: CLT, cross laminated timber, testing, in-plane loading, beam, hole, notch

ACKNOWLEDGMENTS

The work presented in this report was carried out during 2016/2017. The experimental work was carried out at the Division of Structural Mechanics at Lund University during the fall of 2016 while most of the work with evaluation and compilation of test results was carried out during the winter and spring of 2017.

The financial support from the Swedish Research Council Formas through grant 2016-01090 for the project *Cross Laminated Timber Beams - Rational Structural Analysis* is gratefully acknowledged. The financial support from COST Action FP1402 related to the the Short Term Scientific Mission (STSM) for Mario Jelec and his research visit to Lund during the fall of 2016 is also gratefully acknowledged.

We would further like to thank research engineer Per-Olof Rosenkvist at the Division of Structural Engineering for excellent help and much appreciated contributions during the experimental work and also Jonas Engqvist at the Division of Solid Mechanics for helping us out with measurements relating to Digital Image Correlation.

June 2017

Henrik Danielsson, Mario Jelec and Erik Serrano

Contents

1	Introduction	1
2	Test setups and materials	2
2.1	Test series and setups	2
2.2	Test procedure and measurements	8
2.3	Moisture content and density	10
3	Analytical beam models	12
3.1	General assumptions	12
3.2	Prismatic beam	14
3.2.1	Bending	14
3.2.2	Shear mode I and mode II	15
3.2.3	Shear mode III	19
3.3	Beam with a hole	29
3.3.1	Bending	30
3.3.2	Tension perpendicular to beam axis	31
3.3.3	Shear mode I	31
3.3.4	Shear mode II	32
3.3.5	Shear mode III	32
3.4	Beam with an end-notch	33
3.4.1	Bending	34
3.4.2	Tension perpendicular to beam axis	34
3.4.3	Shear mode I	34
3.4.4	Shear mode II	35
3.4.5	Shear mode III	35
3.5	Stiffness	36
3.5.1	Bending stiffness	36
3.5.2	Shear stiffness	37
4	Results	39
4.1	Beam strength	39
4.2	Shear stiffness	52
4.3	Bending stiffness	55
5	Concluding Remarks	58
5.1	Remarks on beam strength	58
5.2	Remarks on beam stiffness	60
5.3	Remarks on analytical beam models	60
	References	61

1 INTRODUCTION

This report concerns investigations of beam strength and stiffness for in-plane beam loading of CLT elements, including prismatic beams and beams with holes and notches as illustrated in Figures 1 and 2. In-plane beam loading of CLT is very relevant from a practical engineering point of view since the cross layers have a reinforcing effect with respect to stress perpendicular to the beam axis. Due to the general structure of cross laminated timber, the stress state is however very complex and there are many possible modes of failure.

Experimental tests were carried out at Lund University during the fall of 2016. The different test series, test setups, test procedure and material are described in Section 2. Analytical models for evaluation of the stress state in the beams and the beam stiffness are presented in Section 3. The test results are presented in Section 4 and some concluding remarks are then given in Section 5.

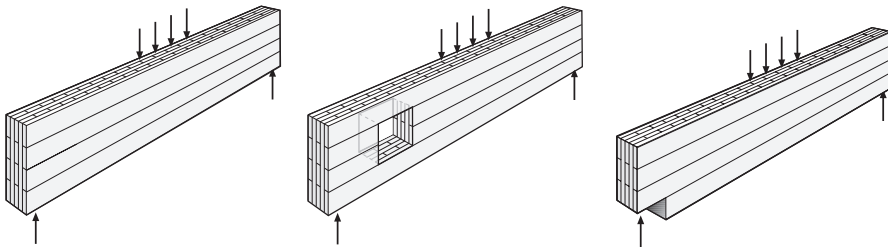


Figure 1: Examples of in-plane beam loading of CLT elements.

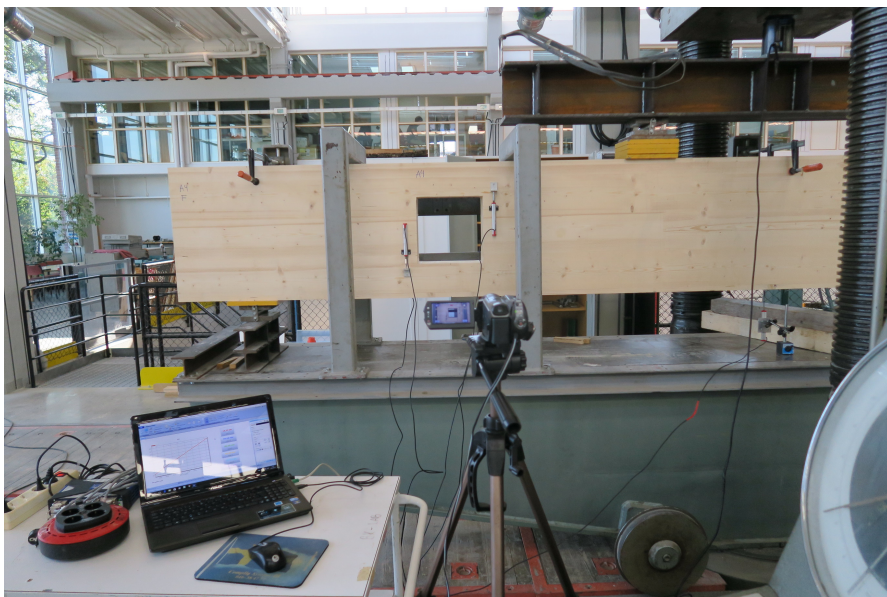


Figure 2: Example of test setup for a beam with a hole.

2 TEST SETUPS AND MATERIALS

2.1 Test series and setups

Five different test setups according to Figure 3 were used. Each test series consisted of four nominally equal tests giving a total of 20 individual tests. Two of the test series concern beams with a hole (test series A and B), one test series concerns beams with an end-notch (test series D) and two test series concern prismatic beams without holes or notches (test series C and E).

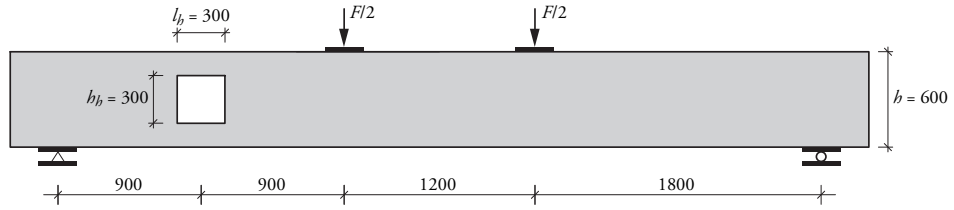
All beams were produced by Cross Timber Systems LTD according to the European Technical Assessment ETA-15/0906 [7]. The wood species used is stated as being European spruce or equivalent softwood. The individual boards are declared as being jointed in the longitudinal directions by finger joints according to EN 14080 [5] to make up continuous laminations having a minimum length of the corresponding dimension of the CLT panel. It is in the ETA stated the the cover layers are composed of laminations corresponding to minimum strength class C24 while the inner layers may be composed of up to 10 % of the laminations corresponding to strength class C16, with strength class properties as defined in EN 338 [3]. The laminations of the different layers are glued together on their flat sides using a formaldehyde-free PUR adhesive. It is in the ETA stated that the narrow faces of the laminations belonging to the same layer need not to be bonded together. At the time of testing, there were no visible gaps between the laminations in the elements used for testing and there appear not to have been any (or very little) edge-bonding between the laminations.

The nominal cross section dimensions were equal for all beams, with a beam height of 600 mm and a beam width of 160 mm. The same element layup, i.e. the number of crosswise bonded layers and thickness of the respective layers, was used for all beams. The element layup is by the producer denoted CLT 160 5L and is composed of three longitudinal layers having a thickness of 40 mm respectively and two transversal layers having a thickness of 20 mm respectively. The laminations used for the longitudinal and transversal layers had a width of 172 mm and 146 mm, respectively.

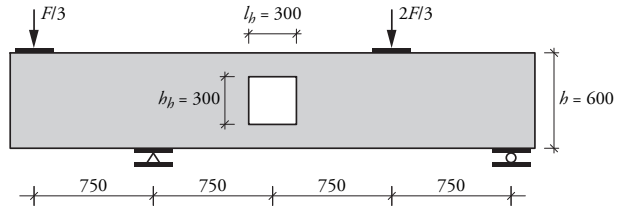
The individual beam elements were cut from larger CLT panels without consideration of the position of the individual laminations in relation to element edges, holes or notches. The number and position of the laminations within the beam elements hence varied between the different individual test specimens, also within a single test series. The cross section dimensions of the individual laminations were measured for all beams, see Figures 4-7. As can be noted from these figures, small deviations compared to the nominal dimensions regarding the total beam height and hole/notch geometry were found.

For test series A and B, a square hole of side length 300 mm was placed centrally with respect to the beam height direction. For test series A, the hole is placed in a position exposed to a combined state of shear force and bending moment loading. For test series B, the hole is placed with its center in a position of zero bending moment and hence a pure shear state of loading. For the test series with end-notched beams, test series D, a notch of depth 300 mm was used.

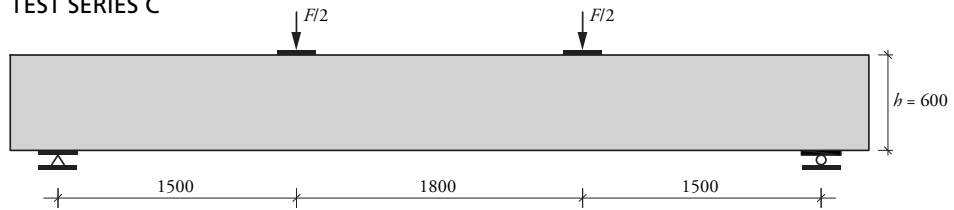
TEST SERIES A



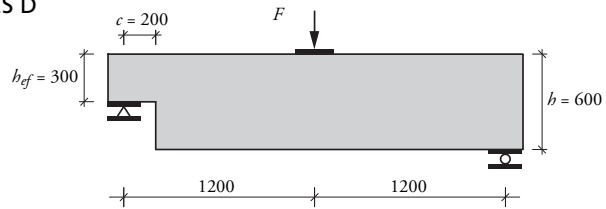
TEST SERIES B



TEST SERIES C



TEST SERIES D



TEST SERIES E

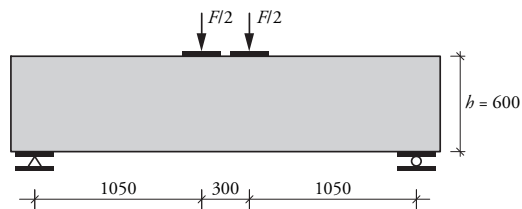


Figure 3: Test setups, dimensions in mm.

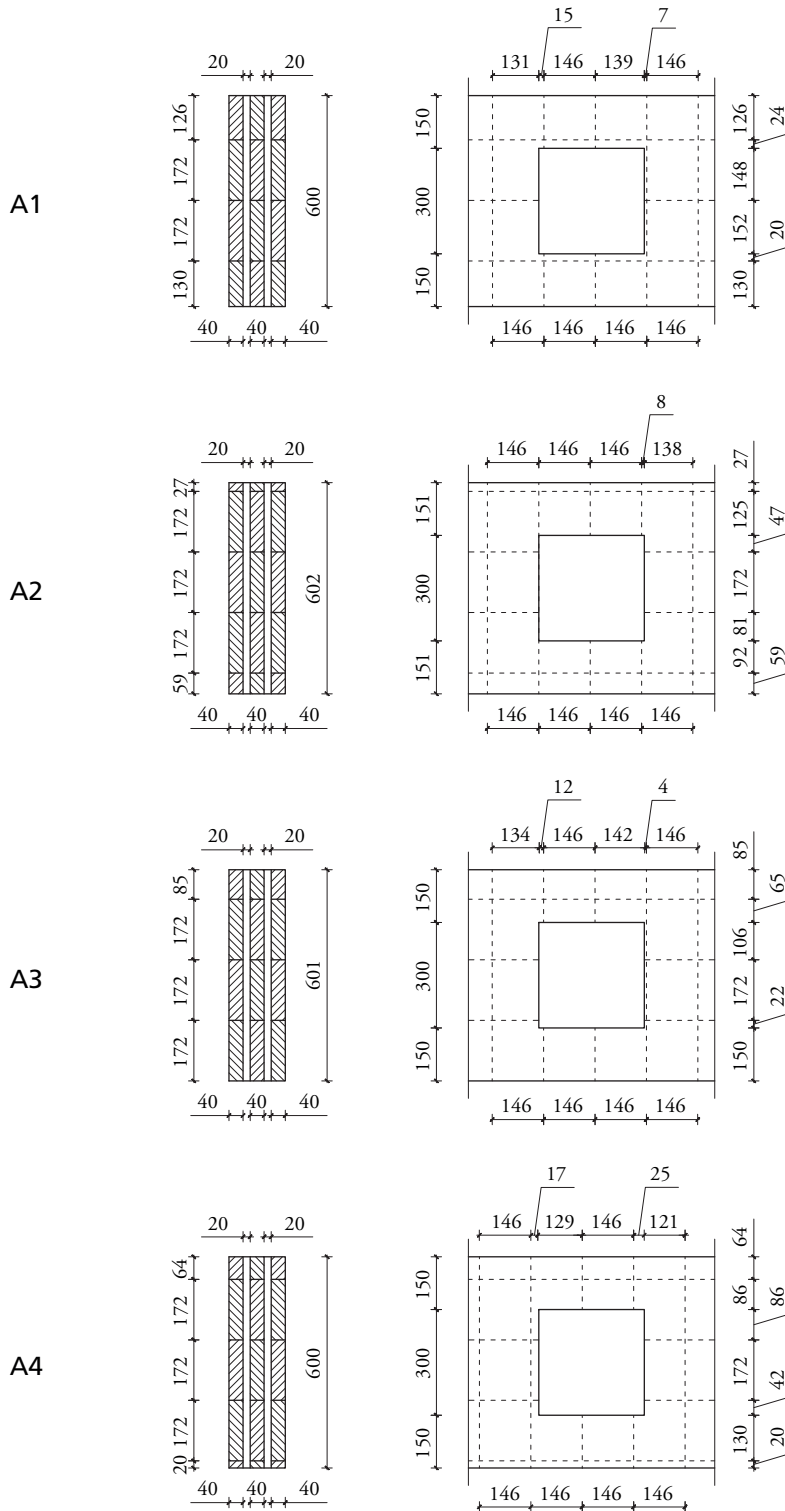


Figure 4: Specimen cross section and lamination dimensions, in mm, for test series A.

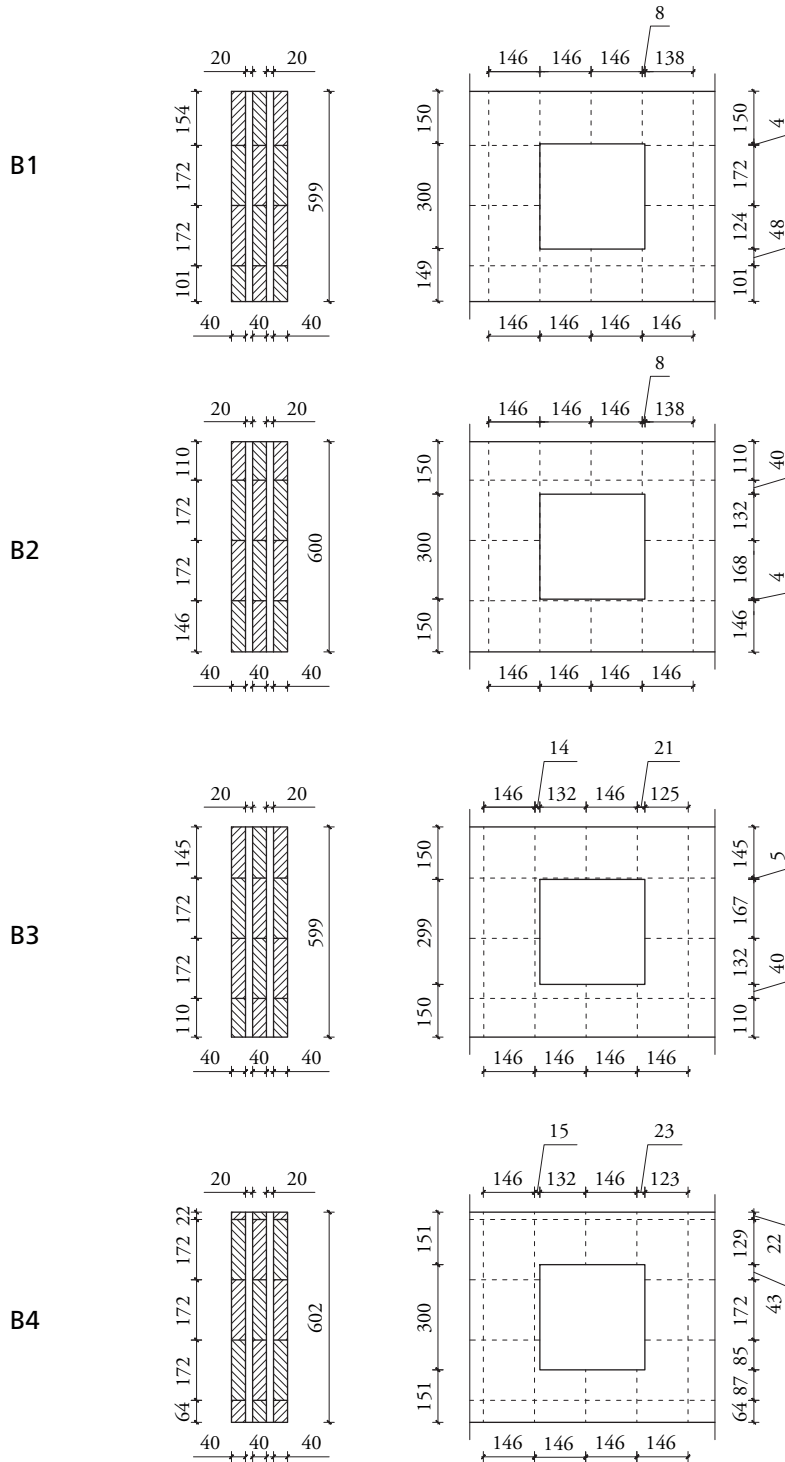


Figure 5: Specimen cross section and lamination dimensions, in mm, for test series B.

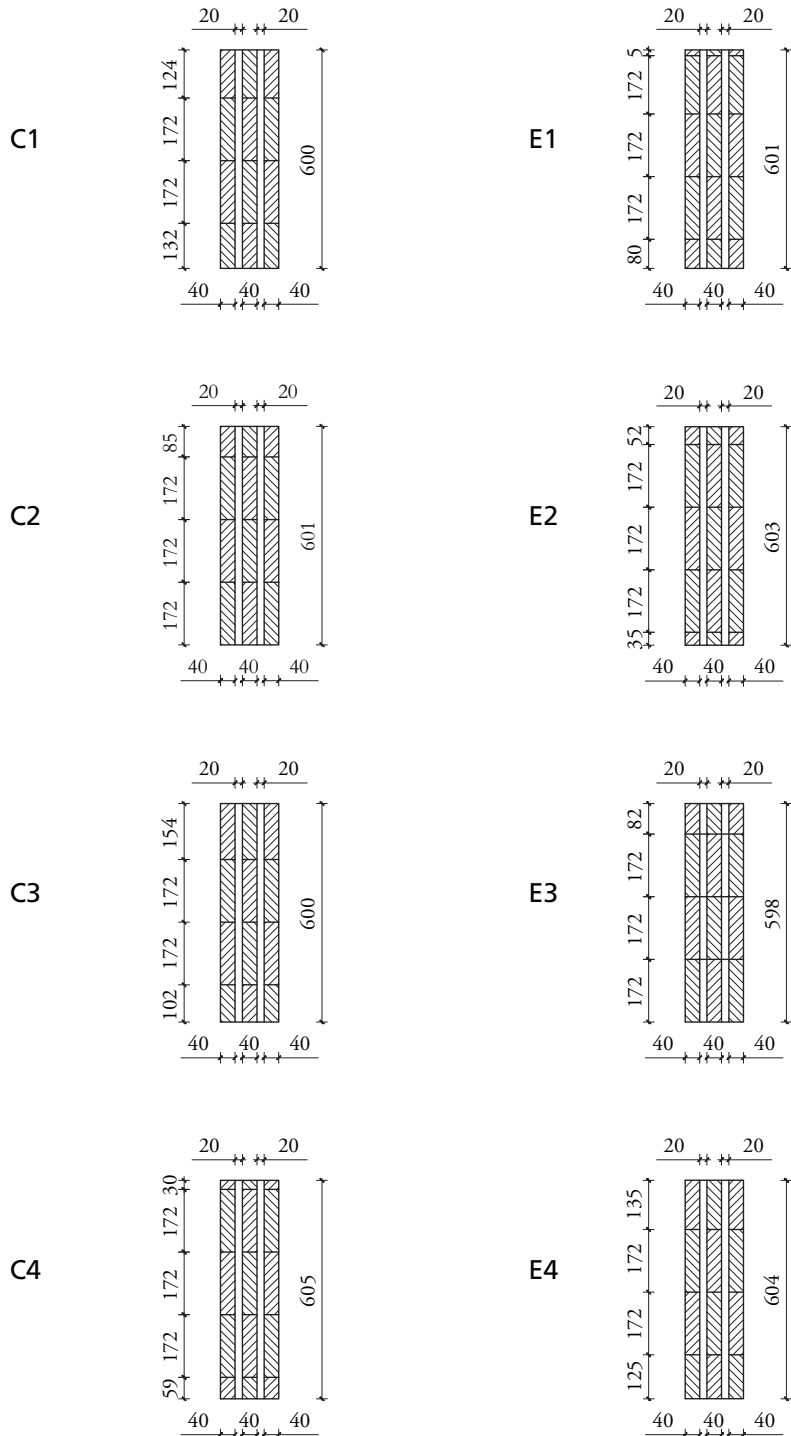


Figure 6: Specimen cross section and lamination dimensions, in mm, for test series C and E.

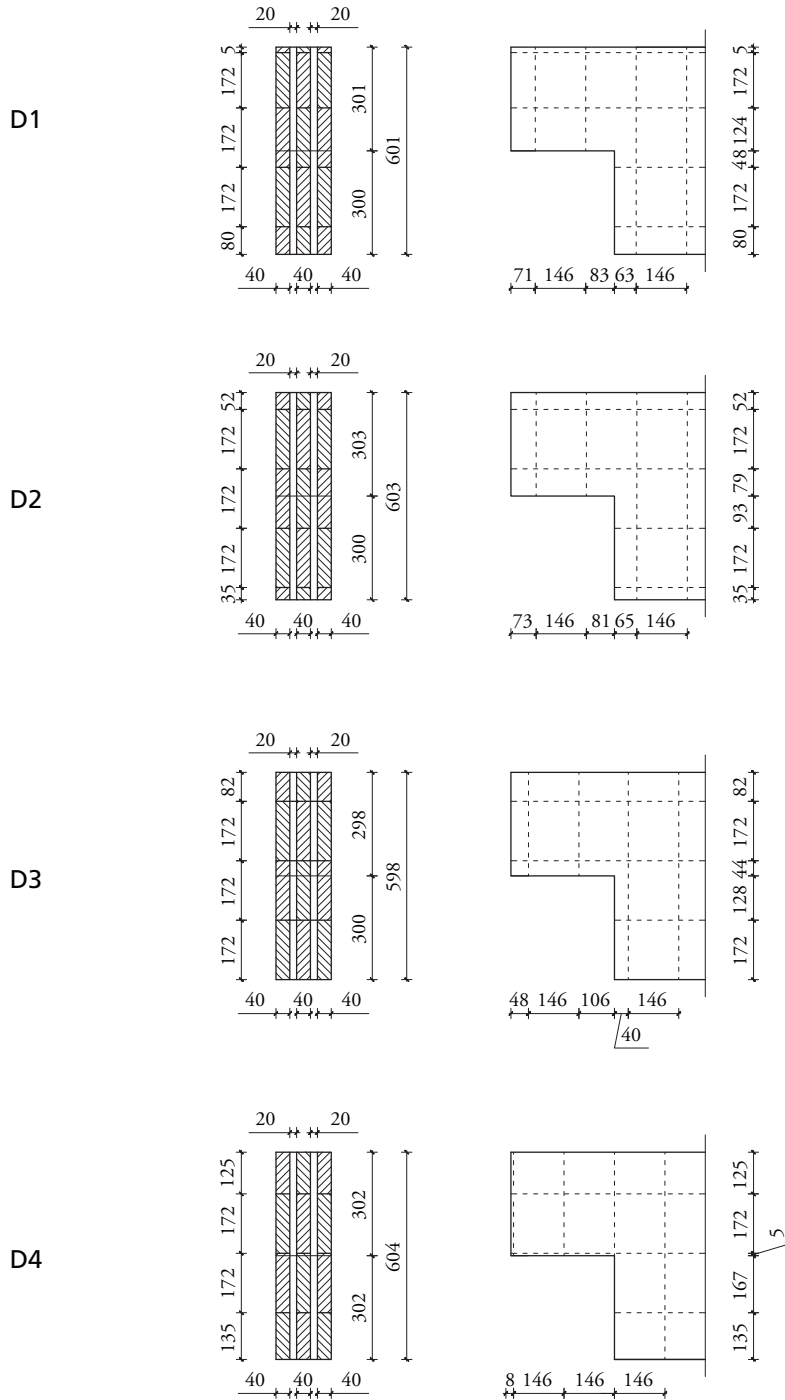


Figure 7: Specimen cross section and lamination dimensions, in mm, for test series D.

2.2 Test procedure and measurements

All tests were run in a deformation controlled manner. The rate of deformation was 0.03 mm/s for test series A and C, while for test series B and E the rate of deformation was 0.02 mm/s and for test series D the rate of the deformation was 0.01 mm/s. The chosen rates of deformation resulted in test durations of approximately 15-20 minutes for each test. The rate of deformation referred to is the rate of the actuator in the testing machine. The rates of deformation were chosen to allow for careful observations of critical corners of holes and notches and other locations on the specimens where cracks were expected during testing. However, cracking in internal laminations and debonding between laminations, not visible by the naked eye, probably also occurred during testing before reaching maximum load for many of the tested specimens. Indications of internal damage of these types were given by sounds of cracking without visible damage to the external laminations and by more or less sudden changes in the recorded load levels and/or in recorded deflections/deformations.

A steel beam (HEB 280) was used for test series A, B and C according to the illustrations shown in Figure 8 in order to achieve the desired loading situations. For load distribution purposes, steel plates were used at all beam supports and load introduction points. The steel plates covered the complete beam width and had a length of 230 mm in the beam length direction. A number of potentiometers were used during testing to measure local deformations and deflection of the beams. Positions and numbering of the devices are shown schematically in Figure 8.

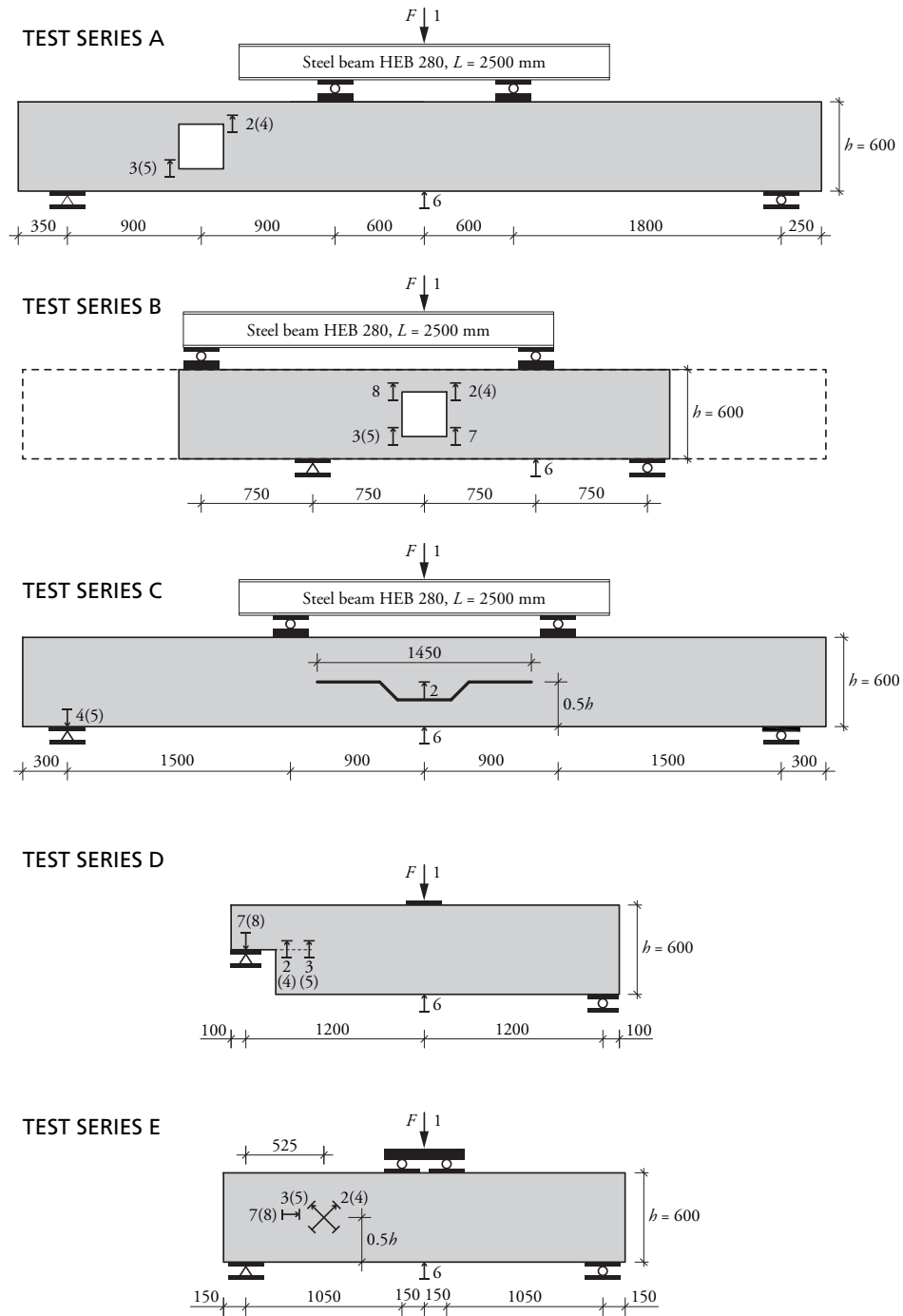


Figure 8: Test arrangement and position of measurement devices, dimensions in mm.

2.3 Moisture content and density

Measurements of moisture content were made on all beams at the time of delivery to Lund University and also at a time after all tests were performed, approximately 12 weeks later. At both occasions, moisture measurements were performed using an electrical resistance type of moisture meter. The beams were kept in an indoor climate of approximately 20°C and 35 % relative humidity from the time of delivery to the time of testing. At the time of delivery, moisture content measurements were done in the central longitudinal layer at three different locations along the beam length. The mean value of three such measurements on the individual beams are given in Table 1 as u_1 . The eight specimens used for test series D and E were cut from four beams of about twice the length of the specimens used for these two test series. Specimen D1 and E1 were cut from the same beam, specimen D2 and E2 from the same beam and so on. The first moisture content measurements were performed before cutting these four beams into two parts, and the moisture contents given in Table 1 for test series E hence reflect average values of the pairs of specimens used for test series D and E.

After testing, a small sample was cut from each beam. The samples were all cut through the entire beam width and had extensions in the beam length and height directions of 80 mm respectively. Moisture content measurements were done on all three longitudinal layers of the small samples using the electrical resistance moisture meter and the results of the mean value of these three measurements on the individual samples are given in Table 1 as u_2 . The cut-out samples were weighted and then left to dry at a temperature of 105°C, until the mass was constant and the moisture content was considered to be zero. The density ρ and the moisture content u of the samples were then determined according

$$\rho = \frac{m_{wet}}{V} \quad (1)$$

and

$$u = \frac{m_{wet} - m_{dry}}{m_{dry}} \quad (2)$$

where V is the sample volume, m_{wet} is the mass of the sample before drying and m_{dry} is the dry mass of the sample. Calculated values of density ρ and moisture content u are presented in Table 1.

Table 1: Moisture content and density.

Specimen	u_1 [%]	u_2 [%]	m_{wet} [g]	ρ [kg/m ³]	m_{dry} [g]	u [%]
A1	10.9	9.5	453.0	442	411.8	10.0
A2	11.0	9.4	450.2	440	409.1	10.0
A3	10.2	10.0	450.5	440	408.2	10.4
A4	11.0	9.8	483.8	472	439.4	10.1
B1	11.0	10.2	480.6	469	433.0	11.0
B2	11.6	10.2	463.1	452	417.3	11.0
B3	11.6	9.6	471.3	460	428.6	10.0
B4	11.0	9.7	437.6	427	397.0	10.2
C1	11.2	9.4	483.5	472	439.9	9.9
C2	11.0	9.9	466.3	455	423.0	10.2
C3	10.4	9.8	479.1	468	435.1	10.1
C4	11.0	9.7	476.0	465	432.0	10.2
D1	10.9	9.9	526.1	514	476.6	10.4
D2	10.7	9.4	469.7	459	426.2	10.2
D3	10.1	9.4	442.1	432	402.6	9.8
D4	10.8	9.7	457.3	447	414.1	10.4
E1	-	9.8	471.6	461	427.8	10.2
E2	-	8.9	474.7	464	430.8	10.2
E3	-	10.2	469.7	459	424.6	10.6
E4	-	10.2	434.3	424	394.9	10.0
mean	10.9	9.7	467	456	424	10.2
std	0.41	0.33	21	20	18	0.32
cov	3.8 %	3.4 %	4.4 %	4.4 %	4.3 %	3.1 %

3 ANALYTICAL BEAM MODELS

3.1 General assumptions

The cross-wise composition of longitudinal and transversal layers gives a far more complex distribution of internal forces and stresses compared to conventional timber, glued laminated timber and laminated veneer lumber elements loaded in bending. CLT elements may further be produced with or without so called edge-bonding (or narrow-face bonding), i.e. gluing of the narrow faces of adjacent laminations within the same layer, which also needs to be taken into account in modeling. According to the European standard EN 16351:2015 [6], significant gaps between laminations in a layer and grooves within a lamination are also allowed. CLT is hence not only strongly heterogeneous in terms of the wood material itself and its principal material directions, but it also includes severe discontinuities.

There are a large number of geometry parameters that influence the stress distribution and hence the beam strength and stiffness. The notation used for geometry parameters, forces, moments and stress components typically differs between different sources such as research reports and articles, ETAs and design handbooks. The notation used for the basic geometry and load parameters in this report is according to Figure 9, and other parameters are defined in the text and the figures found below.

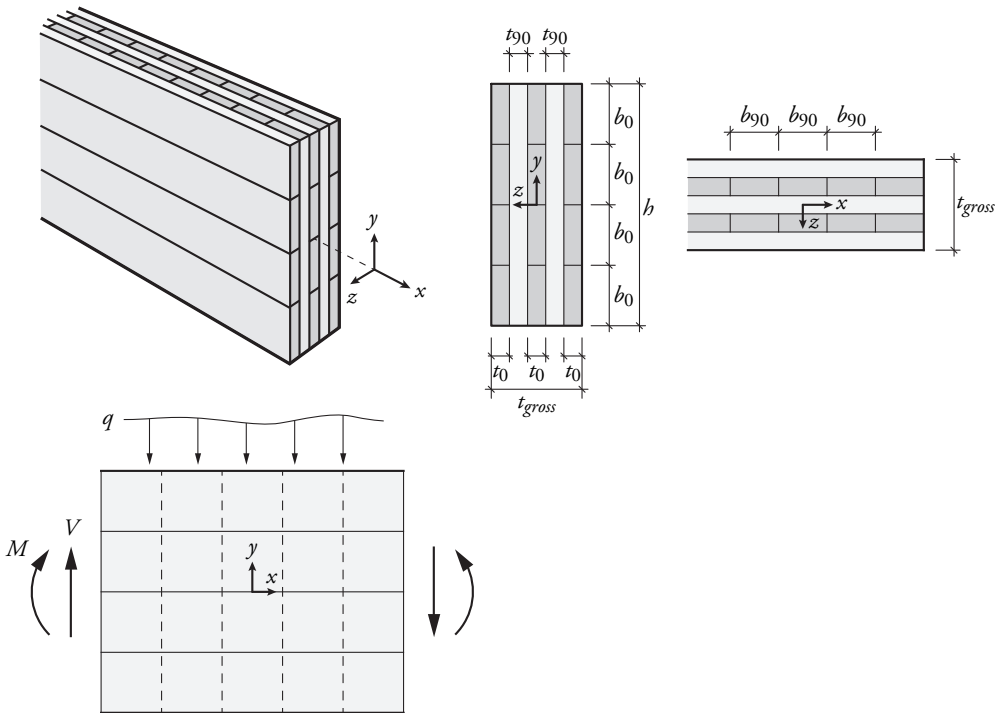


Figure 9: Definitions of geometry and load parameters.

Many of the geometry parameters are for a specific type of CLT element defined by the producer, e.g. the widths t_0 and t_{90} of the longitudinal and transversal layers respectively. Other parameters, such as dimensions of individual laminations and lamination placement with respect to element edges and edges of holes and notches, are often not known to the engineer in an actual design situation since the CLT beams in general are cut from larger elements. In this cutting, no consideration of the location of the beam element edges in relation to the edges of the individual laminations is done. Laminations width b_0 and b_{90} are in ETAs commonly stated as an interval, with a typically range of 80 – 250 mm for both the longitudinal and transversal layers. The lamination cross section ratios b_0/t_0 and b_{90}/t_{90} are commonly also stated.

Models for stress analysis and models for calculation of beam strength and stiffness for in-plane loading of CLT elements are for example found in [8], [9] and [10]. These models are in general based on conventional beam theory considerations with addition of certain assumptions and simplifications to account for the orthogonal layered composition and are furthermore aimed at arriving at reasonably convenient equations that can be used in practical design situations. The models presented in [8], [9] and [10] and some other models for strength and stiffness analysis are reviewed in the sections below. A basic assumption is that normal stress in the plane of the element is only carried by the layers that are oriented with the grain direction parallel to the stress direction. This assumption is motivated by the large difference in stiffness between parallel and perpendicular to grain loading directions, with $E_0/E_{90} \approx 15 - 35$.

Recommendations for practical design, found in design handbooks and producer ETAs, are not always in total agreement both in terms of notation used and models for stress and strength analysis. It should especially be noted that the notation of failure mode I, II and III for the three different types of shear related failures as gross shear failure (FM I), net shear failure (FM II) and failure in the crossing areas (FM III) is not consistent in the literature.

3.2 Prismatic beam

3.2.1 Bending

For calculation of normal stress parallel to the beam axis, the conventional beam theory assumption that plane cross sections initially perpendicular to the beam axis remain plane and perpendicular to the beam axis during deformation is used. The normal strain distribution is assumed to have a linear variation over the beam height and any shear slip between adjacent longitudinal laminations within the same layer is hence neglected. The normal stress in the transversal layers is assumed to be zero and the normal stress in the longitudinal laminations are assumed to be constant with respect to the beam width direction. The normal stress σ_x in the longitudinal layers due to bending is then given by

$$\sigma_x = -\frac{M}{I_{net}}y \quad \text{where} \quad I_{net} = \frac{t_{net,0}h^3}{12} \quad (3)$$

and the maximum value of the normal stress is given by

$$\sigma_{x,max} = \frac{M}{W_{net}} \quad \text{where} \quad W_{net} = \frac{t_{net,0}h^2}{6} \quad (4)$$

where M is the bending moment, I_{net} and W_{net} are the second moment of inertia and the elastic section modulus, respectively, considering the net cross section of the longitudinal layers, $t_{net,0} = \sum t_{0,i}$ is the net cross section width considering the longitudinal layers only and h is the beam height.

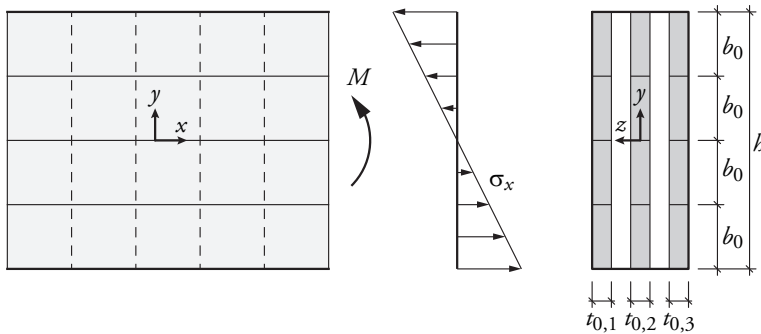


Figure 10: Illustration of normal stress distribution due to bending.

3.2.2 Shear mode I and mode II

Schematic illustrations of shear stress distributions in the longitudinal and transversal layers are presented in Figure 11, which is based on [8]. The shear stress in the longitudinal layers is here denoted $\tau_{xy,0}$ and the shear stress in the transversal layers is denoted $\tau_{xy,90}$. The shear stress within each lamination is assumed to be constant with respect to the beam element width (z) direction. For a given location in the beam length and height directions, equal shear stress $\tau_{xy,0}$ is assumed for the laminations of the longitudinal layers and equal (but in general different from $\tau_{xy,0}$) shear stress $\tau_{xy,90}$ is assumed for the laminations of the transversal layers. The illustrations are based on assuming no edge-bonding but still having zero size of the gap between adjacent laminations of the same layer. Zero friction between adjacent laminations of the same layer is further assumed, meaning that the shear stress in the laminations must be zero at the interface between two individual laminations within the same layer.

The illustrations in Figure 11 relate to a beam composed of longitudinal layers which all have four laminations ($m = 4$) of identical lamination width ($b = b_0$) in the beam height direction. The width of the longitudinal layers is further assumed as twice the width of the transversal layers, i.e. $t_0 = 2t_{90}$. Section A-A relate to a location in the beam length direction corresponding to a section through the center of a transversal lamination while section B-B relate to a location corresponding to the interface between adjacent transversal laminations.

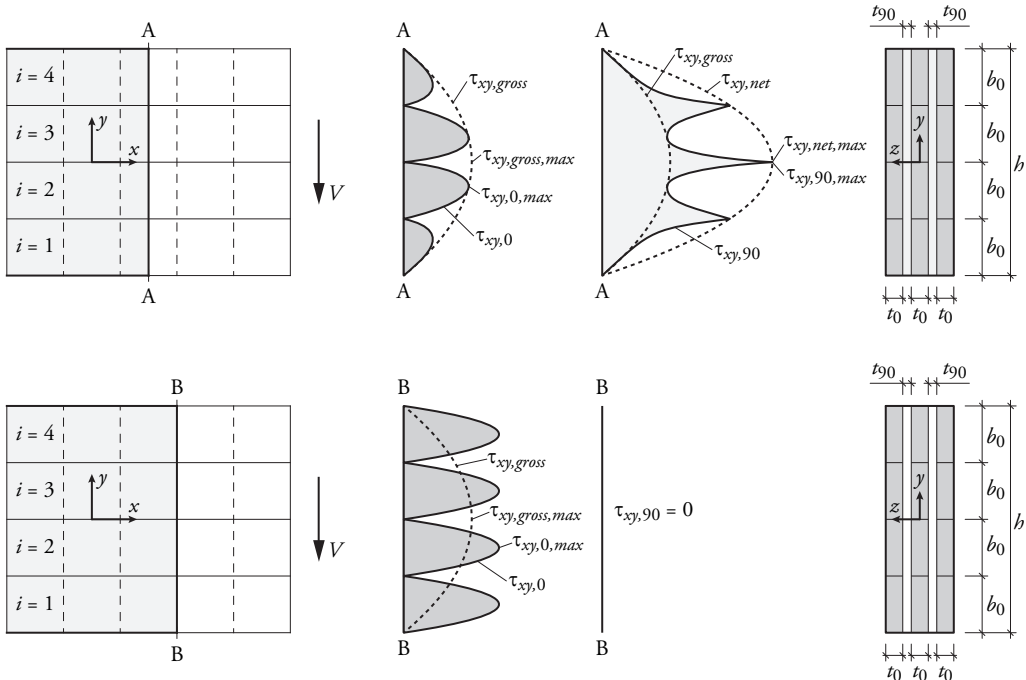


Figure 11: Illustration of shear stress distribution in longitudinal (left) and transversal (right) layers for a beam width four laminations in the beam height direction.

A gross shear stress distribution $\tau_{xy,gross}$, related to the gross cross section of the beam, is defined according to

$$\tau_{xy,gross} = \frac{VS_{gross}}{I_{gross}t_{gross}} \quad (5)$$

where S_{gross} is the static moment of area considering the gross cross section, I_{gross} is the second moment of inertia considering the gross cross section and t_{gross} is the beam gross cross section width. The maximum value of the gross shear stress is then given by

$$\tau_{xy,gross,max} = \frac{3}{2} \frac{V}{t_{gross}h} \quad (6)$$

corresponding to the maximum value of the beam theory shear stress distribution for a homogeneous cross section of width t_{gross} and height h . For section A-A, corresponding to a location through the center of a transversal lamination, the shear stress $\tau_{xy,0}$ in the two outermost longitudinal laminations ($i = 1$ and $i = 4$) and the shear stress $\tau_{xy,90}$ in the transversal laminations are assumed to follow the parabola defined by the gross shear stress $\tau_{xy,gross}$ close to the upper and lower edge of the beam.

For locations in the beam height direction corresponding to the interfaces between adjacent longitudinal laminations, i.e. for $y = -b_0, 0$ and b_0 in Figure 11, the shear stress in the longitudinal layers must be zero (due to equilibrium) and the entire shear flow in the beam must instead be carried by the transversal laminations. The values of the shear stress $\tau_{xy,90}$ in the transversal layers at these locations are hence found on the parabola defined by a net shear stress $\tau_{xy,net}$ according to

$$\tau_{xy,net} = \frac{VS_{net}}{I_{net}t_{net,90}} \quad (7)$$

where S_{net} is the static moment of area considering the net cross section of the longitudinal layers, I_{net} is the second moment of inertia considering the net cross section of the longitudinal layers and $t_{net,90}$ is the beam net cross section width considering the transversal layers, i.e. $t_{net,90} = 2t_{90}$ for the beam in Figure 11. The maximum value of the shear stress $\tau_{xy,90}$ in the transversal laminations is hence given by

$$\tau_{xy,90,max} = \tau_{xy,net,max} = \frac{3}{2} \frac{V}{t_{net,90}h} \quad (8)$$

for the present case with an even number of longitudinal laminations in the beam height direction.

At section B-B, i.e. at the interface between adjacent transversal laminations within the same layer, the entire shear force must be carried by the longitudinal laminations. Assuming that the total shear force V is divided evenly between the longitudinal laminations according to $V_i = V/m$ and further that the shear stress distribution is parabolic within each lamination, the maximum shear stress in the longitudinal laminations is given by

$$\tau_{xy,0,max} = \frac{3}{2} \frac{V_i}{t_{net,0}b_0} = \frac{3}{2} \frac{V}{t_{net,0}h} \quad (9)$$

where $t_{net,0}$ is the beam net cross section width considering the longitudinal layers only, i.e. $t_{net,0} = 3t_0$ for the beam in Figure 11. At this location, the shear stress in the transversal laminations is zero due to the assumption of no edge-bonding and zero friction between adjacent laminations.

For the beam geometry illustrated in Figure 11 above, with longitudinal layers composed of an even number m laminations in the beam height direction, and for the assumed stress distributions, the maximum value of the shear stress in the transversal laminations is exactly equal to the maximum value of the net shear stress, i.e. $\tau_{xy,90,max} = \tau_{xy,net,max}$. At locations corresponding to section A-A, the maximum value of the shear stress in the longitudinal laminations is approximately, but not exactly, equal to the maximum value of the gross shear stress, i.e. $\tau_{xy,0,max} \approx \tau_{xy,gross,max}$. For beam geometries with longitudinal layers composed of an uneven number of laminations m , for example with $m = 3$ as illustrated in Figure 12, the situation is slightly different. For uneven m , the maximum value of the shear stress in the longitudinal laminations is at section A-A exactly equal to the maximum value of the gross shear stress, i.e. $\tau_{xy,0,max} = \tau_{xy,gross,max}$. The value of the maximum shear stress in the transversal layers is then instead only approximately equal to the maximum value of net shear stress, i.e. $\tau_{xy,90,max} \approx \tau_{xy,net,max}$. The maximum value of the shear stress in the longitudinal layers, found at section B-B, is however according to the assumed stress distributions the same irrespective of m being even or uneven.

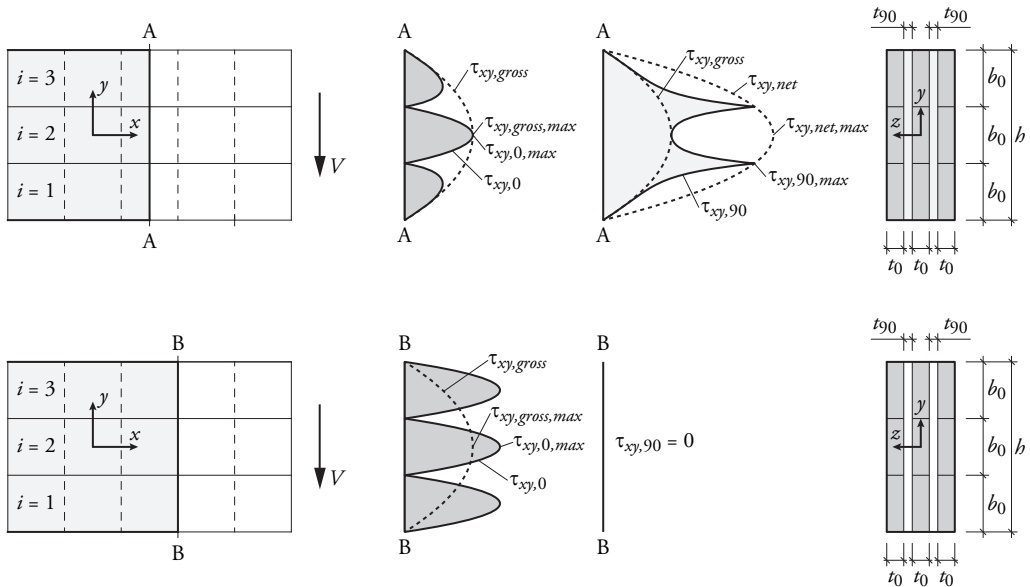


Figure 12: Illustration of shear stress distribution in longitudinal (left) and transversal (right) layers for a beam width three laminations in the beam height direction.

Based on the assumed stress distributions according to Figures 11 and 12, expressions for the exact values of the maximum shear stress in the longitudinal and transversal layers at a location corresponding to section A-A are given below. The maximum value of the shear stress in the transversal layers can for different values of m be expressed as

$$\tau_{xy,90,max} = \begin{cases} \frac{3}{2} \frac{V}{t_{net,90}h} & \text{for } m = 2, 4, 6, \dots \\ \frac{3}{2} \frac{V}{t_{net,90}h} \frac{m^2 - 1}{m^2} & \text{for } m = 3, 5, 7, \dots \end{cases} \quad (10)$$

and the value of the shear stress in the center of the two most centrally, with respect to the beam height direction, placed longitudinal layers at section A-A can for different values of m be expressed as

$$\tau_{xy,0,max} = \begin{cases} \frac{3}{2} \frac{V}{t_{gross}h} \frac{m^2 - 1}{m^2} & \text{for } m = 2, 4, 6, \dots \\ \frac{3}{2} \frac{V}{t_{gross}h} & \text{for } m = 3, 5, 7, \dots \end{cases} \quad (11)$$

Ratios between maximum shear stresses as influenced by the number of laminations in the longitudinal layers m are presented in Table 2. The maximum shear stresses $\tau_{xy,90,max}$ and $\tau_{xy,0,max}$ are calculated based on Equations (10) and (11) respectively while stresses $\tau_{xy,gross,max}$ and $\tau_{xy,net,max}$ are based on Equations (6) and (8).

Table 2: Ratio of shear stress components for locations corresponding to section A-A.

m	2	3	4	5	6	7	8	9	10
$\tau_{xy,0,max}/\tau_{xy,gross,max}$	0.75	1.00	0.94	1.00	0.97	1.00	0.98	1.00	0.99
$\tau_{xy,90,max}/\tau_{xy,net,max}$	1.00	0.89	1.00	0.96	1.00	0.98	1.00	0.99	1.00

Shear failure modes I and II are commonly referred to as *gross shear failure* and *net shear failure* respectively. The stress components used for evaluation of test results in this report are

$$\tau_{xy,gross} = \frac{3}{2} \frac{V}{t_{gross}h} \quad (12)$$

$$\tau_{xy,0} = \frac{3}{2} \frac{V}{t_{net,0}h} \quad (13)$$

$$\tau_{xy,90} = \frac{3}{2} \frac{V}{t_{net,90}h} \quad (14)$$

where $\tau_{xy,gross}$ is relevant for FM I while $\tau_{xy,0}$ and $\tau_{xy,90}$ are relevant for FM II.

3.2.3 Shear mode III

For in-plane loading of CLT beam elements, shear stress τ_{xz} and τ_{yz} acting in the crossing areas between transversal and longitudinal laminations arise in addition to the shear stresses τ_{xy} which are present in both the longitudinal and transversal layers. Using a composite beam model as suggested in [8], the shear stresses acting in the crossing area can be categorized as

- (1) shear stress parallel to the beam axis τ_{xz} ,
- (2) shear stress perpendicular to the beam axis τ_{yz} and
- (3) torsional shear stress τ_{tor} .

In the crossing areas, these shear stress components represent at the same time both longitudinal and rolling shear stress in the longitudinal and transversal laminations respectively. The basic considerations of the derivation of the shear stress components acting in the crossing areas between longitudinal and transversal laminations are reviewed below, using notation and definitions according to Figures 13 and 14.

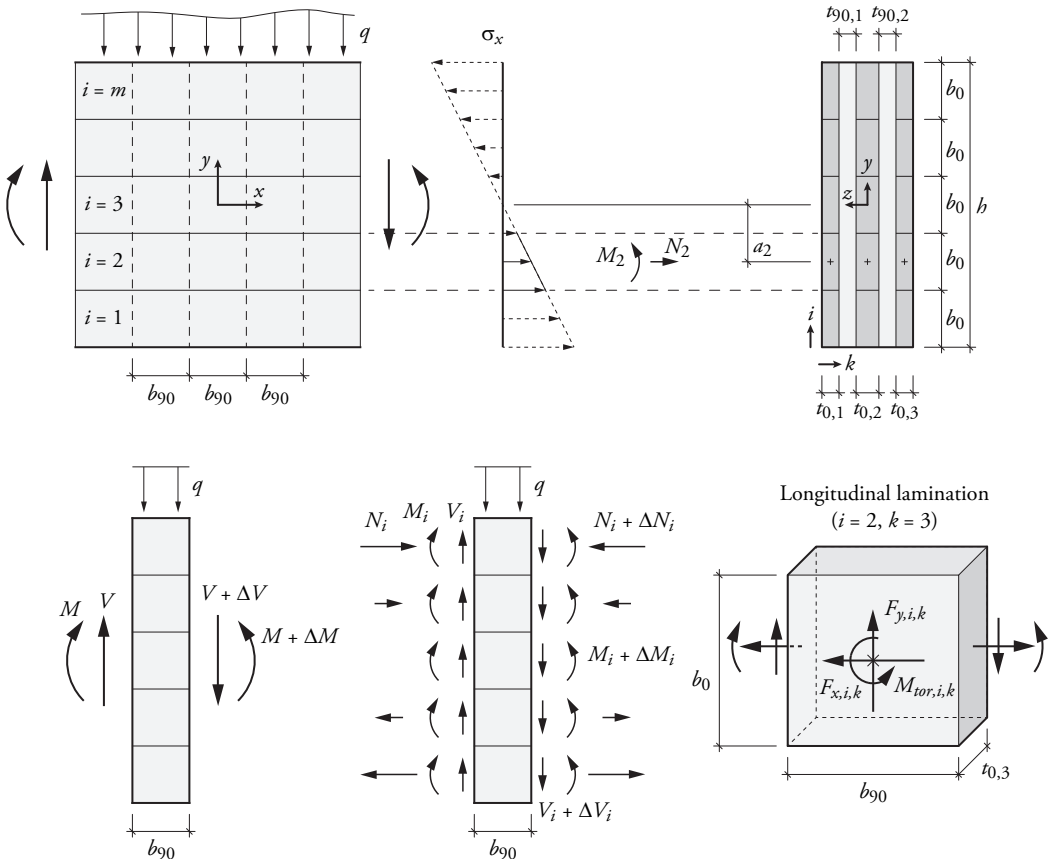


Figure 13: Illustration of composite beam model used for derivation of the shear stresses acting in the crossing areas.

In general, the laminations of the longitudinal layers are assumed to be of width b_0 while the laminations of the transversal layers are assumed to be of width b_{90} . Index $i = 1, \dots, m$ represent the position of the longitudinal laminations in the beam height (y) direction and index $k = 1, 2, 3, \dots$ represent the position of the longitudinal layers in the beam width (z) direction. All laminations are assumed to have identical elastic stiffness properties. The parallel to beam axis normal stress distribution in the longitudinal layers is furthermore assumed to be constant with respect to the beam width (z) direction and assumed to have a linear variation in the beam height (y) direction. The parallel to beam axis normal stress is assumed to be zero in the transversal laminations.

The axial force N_i and the bending moment M_i refer to the total force and the total bending moment, respectively, acting in all laminations i , i.e. in all longitudinal laminations in the beam width direction at a certain position in the beam height direction. The shear force V_i refers likewise to the force in all laminations i at a location in the beam length direction corresponding to an interface between adjacent transversal laminations within the same layer. Since the upper and lower surface of each longitudinal lamination is assumed to be traction-free, the differential forces and moments acting on a part of a single longitudinal lamination of length b_{90} must be balanced by corresponding shear stresses in the crossing areas between the considered longitudinal lamination part and its neighboring transversal lamination/laminations.

If nothing else is explicitly stated, the presentation below relates to the case of a CLT beam element composed of transversal laminations of width b_{90} and longitudinal laminations of width b_0 . The total beam height is $h = mb_0$, with m as an integer. The laminations of the longitudinal and transversal layers are also assumed to be placed in a regular pattern, as illustrated in Figure 13.

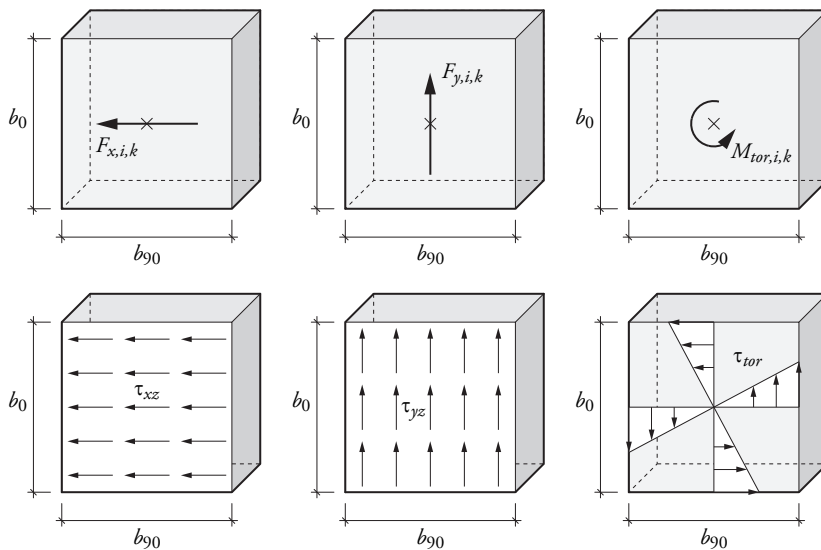


Figure 14: Illustration of assumed shear stress distribution.

Shear stress parallel to beam axis

Shear stress parallel to the beam axis, τ_{xz} , arises due to differential normal forces and are assumed to be evenly distributed over the crossing area between a longitudinal and a transversal lamination, see Figures 13 and 14. The shear stress $\tau_{xz,i,k}$ in the crossing area/areas belonging to lamination i, k , is given by

$$\tau_{xz,i,k} = \frac{F_{x,i,k}}{b_0 b_{90}} = \frac{\Delta N_{i,k}}{b_0 b_{90} n_{CA,k}} \quad (15)$$

where $\Delta N_{i,k}$ is the differential normal force in lamination number i of layer number k , $n_{CA,k}$ is the number of crossing areas that longitudinal lamination i, k shares with adjacent transversal laminations ($n_{CA,k} = 1$ for external layers and $n_{CA,k} = 2$ for internal layers) while b_0 and b_{90} are the lamination widths of the longitudinal and transversal laminations respectively. The differential normal force $\Delta N_{i,k}$ can be expressed as

$$\Delta N_{i,k} = \frac{\Delta M}{I_{net}} t_{0,k} b_0 a_i \quad (16)$$

where a_i is the distance in the y -direction from the center-line of the gross cross section to the center-line of lamination i, k and where $t_{0,k}$ is the width of longitudinal layer k . Expressing the differential bending moment as $\Delta M = V b_{90}$ and using Equations (15) and (16), the shear stress parallel to the beam axis can be expressed as

$$\tau_{xz,i,k} = \frac{12V}{h^3 n_{CA,k} t_{net,0}} t_{0,k} a_i \quad (17)$$

where V is the total shear force and h is the total beam height.

According to this model, the maximum shear stress parallel to the beam axis is found in the crossing areas of the upper/lower-most longitudinal laminations of the beam, i.e. for $i = 1$ and $i = m$. The maximum value depends also on the element lay-up in terms of the relative widths of the longitudinal layers $t_{0,k}$. The most favorable stress situation is obtained for lay-ups with constant value of $t_{0,k}/n_{CA,k}$ for all longitudinal layers. This condition is always fulfilled for 3-layer elements with symmetric layup while for 5- and 7-layer elements, its only fulfilled when the internal layers have twice the width of the external layers. The shear stress parallel to the beam axis may for constant value of $t_{0,k}/n_{CA,k}$ for all longitudinal layers be expressed as

$$\tau_{xz,i,k} = \frac{12V}{h^3 n_{CA}} a_i \quad (18)$$

where n_{CA} is the total number of crossing areas in the beam width direction. For the case of equal width b_0 for all laminations in the longitudinal layers, the maximum stress according to Equation (17) may also be expressed as

$$\tau_{xz,max} = \frac{6V}{b_0^2 n_{CA}} \left(\frac{1}{m^2} - \frac{1}{m^3} \right) \quad (19)$$

where m is the number of laminations in the beam height direction and hence $h = m b_0$.

According to [8], Equations (18) and (19) give good approximations for the range of lay-ups that are used in practice, also when the ratio $t_{0,k}/n_{CA,k}$ is not constant. Lay-ups with constant value of $t_{0,k}/n_{CA,k}$ for all longitudinal layers are not very common on the market. On the contrary, CLT element lay-ups have more often greater longitudinal layer widths in the outside layers than in the internal layers. Equations (18) and (19) then underestimate the maximum value of the shear stress parallel to the beam axis.

Comparing Equations (17) and (18), the difference in predicted stress in the crossing areas belonging to longitudinal lamination k may be expressed as the factor $(t_{0,k}/t_{net,0}) \cdot (n_{CA}/n_{CA,k})$. The relationship between the relative widths of the internal and external layers and the predicted stress for the respective layers is graphically illustrated in Figure 15 for a 5-layer CLT element. Assuming a fixed total beam net cross section width $t_{net,0}$, the stress increases by 33 % for the common case of equal width of all longitudinal layers and by 60 % for the case of external layers having twice the width of the internal layer compared to the reference case of $t_{0,2}/t_{0,1} = t_{0,2}/t_{0,3} = 2.0$.

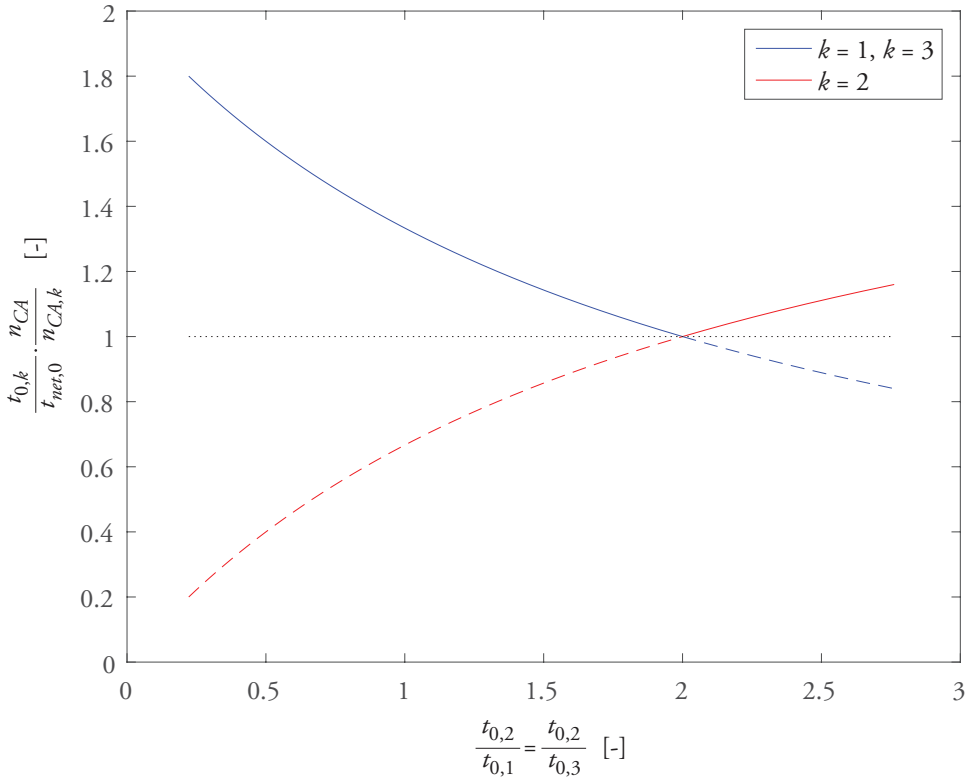


Figure 15: Factor for predicted shear stress vs. relative width of longitudinal layers.

Shear stress perpendicular to beam axis

Shear stress perpendicular to the beam axis, τ_{yz} , arises for example due to transverse loading of the beam by externally applied loads and support reaction forces. Transverse loads are assumed to be introduced in the transversal layers, due to the large difference in stiffness between parallel and perpendicular to grain loading directions. Shear stress perpendicular to the beam axis may also arise due to internal redistribution of forces caused by irregularities in the geometrical shape of the beam, e.g. in the vicinity of a hole or a notch.

Shear stress perpendicular to the beam axis arise due to the differential shear forces and are assumed to be evenly distributed over the crossing area between a longitudinal and a transversal lamination, see Figures 13 and 14. The shear stress $\tau_{yz,i,k}$ in the crossing area/areas belonging to lamination i, k is given by

$$\tau_{yz,i,k} = \frac{F_{y,i,k}}{b_0 b_{90}} = \frac{\Delta V_{i,k}}{b_0 b_{90} n_{CA,k}} \quad (20)$$

where $\Delta V_{i,k}$ is the differential shear force in lamination number i of layer number k , $n_{CA,k}$ is the number of crossing areas that longitudinal lamination i, k shares with adjacent transversal laminations ($n_{CA,k} = 1$ for external layers and $n_{CA,k} = 2$ for internal layers) while b_0 and b_{90} are the widths of the longitudinal and transversal laminations respectively. The differential shear force ΔV_i in laminations i is assumed to be divided between the k laminations in the beam width direction according to

$$\Delta V_{i,k} = \Delta V_i \frac{t_{0,k}}{t_{net,0}} \quad (21)$$

and hence according to the relative widths of the longitudinal layers.

For a beam with constant value of $t_{0,k}/n_{CA,k}$ for all longitudinal layers, composed of m longitudinal laminations in the beam height direction and assuming the total shear force to be evenly divided between the laminations in the beam height direction according to $\Delta V_i = \Delta V/m$, the shear stress perpendicular to the beam axis can be expressed as

$$\tau_{yz} = \frac{\Delta V}{b_0 b_{90} m n_{CA}} \quad (22)$$

where n_{CA} is the total number of crossing areas in the beam width direction. Expressing the differential shear force as $\Delta V = q b_{90}$, the shear stress perpendicular to the beam axis can be expressed as

$$\tau_{yz} = \frac{q}{b_0 m n_{CA}} = \frac{q}{h n_{CA}} \quad (23)$$

where q [N/m] may represent an externally applied distributed load or a distributed support reaction force.

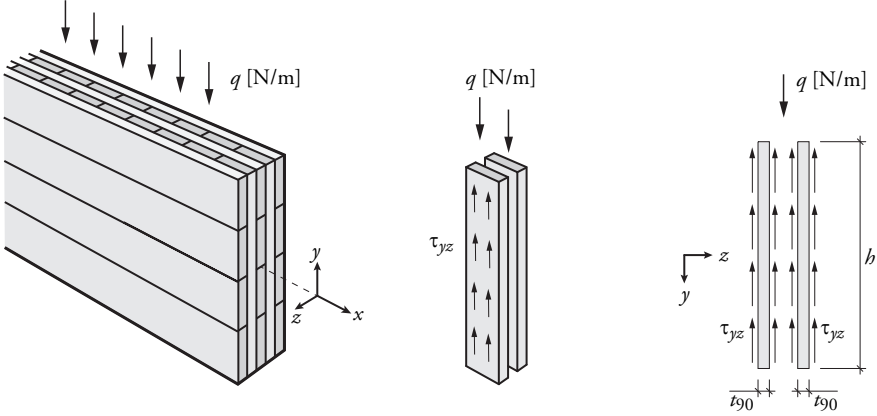


Figure 16: Illustration of shear stress perpendicular to beam axis.

Torsional shear stress

A model for calculation of the torsional moment M_{tor} and related torsional shear stress τ_{tor} acting in the crossing areas between longitudinal and transversal laminations can be derived according to the illustrations in Figures 13 and 14. The derivation as presented in [8], and reviewed below, is based on a number of basic assumptions. Equal width of all laminations in the longitudinal and the transversal layers according to $b_0 = b_{90} = b$ is assumed and the total beam height is assumed as $h = mb$, where m is an integer. The torsional moment M_{tor} and the torsional shear stress τ_{tor} are assumed to be equal for all crossing areas in the beam width direction. These assumptions are in-line with the assumption of equal shear stress parallel to the beam axis τ_{xz} for all crossing areas in the beam width direction irrespective of the element lay-up in terms of the relative widths of the longitudinal layers $t_{0,k}$, discussed above. The torsional moment M_{tor} is further assumed to be equal for all crossing areas in the beam height direction.

Based on these assumptions, the maximum torsional shear stress can according to [8] be expressed as

$$\tau_{tor} = \frac{\sum_{i=1}^m M_{tor,i}}{n_{CA} \sum_{i=1}^m I_{p,CA,i}} \frac{b}{2} \quad (24)$$

where $I_{p,CA,i}$ is the polar moment of inertia for a single crossing area and hence

$$\sum_{i=1}^m I_{p,CA,i} = m \frac{b^4}{6} \quad (25)$$

and where the sum of the torsional moments is given by

$$\sum_{i=1}^m M_{tor,i} = \sum_{i=1}^m (\Delta N_i a_i) = \frac{\Delta M}{I_{net}} t_{net,0} b \sum_{i=1}^m a_i^2 \quad (26)$$

where a_i is the distance in the y -direction from the center-line of the gross cross section to the center-line of lamination i . Expressing the differential bending moment as $\Delta M = Vb$ and using Equations (25) and (26), Equation (24) can be rewritten as

$$\tau_{tor} = \frac{36V}{m^4 b^4 n_{CA}} \sum_{i=1}^m a_i^2 \quad (27)$$

As shown in [8], the summation of the squared distances a_i may for a beam of height $h = mb$ be expressed in closed form as

$$\sum_{i=1}^m a_i^2 = \frac{b^2}{12} (m^3 - m) \quad (28)$$

and the maximum torsional shear stress τ_{tor} can finally be expressed as

$$\tau_{tor} = \frac{3V}{b^2 n_{CA}} \left(\frac{1}{m} - \frac{1}{m^3} \right) \quad (29)$$

The above given relations apply when the basic assumptions stated above are fulfilled. For beams with different lamination widths in the transversal and longitudinal layers, i.e. for $b_0 \neq b_{90}$, but still having consistent laminations widths within the transversal and longitudinal layers respectively, the maximum shear stress is according to [8] given by

$$\tau_{tor} = \frac{3V}{b_0^2 n_{CA}} \left(\frac{1}{m} - \frac{1}{m^3} \right) k_b \quad \text{where} \quad k_b = \frac{b_{max}}{b_0} \frac{2b_0^2}{b_0^2 + b_{90}^2} \quad (30)$$

and where $b_{max} = \max\{b_0, b_{90}\}$.

For the general case of a beam having different widths of the laminations within the longitudinal layers, the torsional shear stress may according to [8] be calculated according to

$$\tau_{tor,i} = \frac{6V b_{90}}{h^3 n_{CA}} \frac{\sum_{i=1}^m (a_i^2 b_{0,i})}{\sum_{i=1}^m I_{p,CA,i}} b_{max,i} \quad (31)$$

where $b_{max,i} = \max\{b_{0,i}, b_{90}\}$.

Accounting also for the uneven distribution of the torsional shear stresses in the beam width direction, due to differences in the ratio $t_{0,k}/n_{CA,k}$ between the k longitudinal layers, the torsional shear stress should be expressed as

$$\tau_{tor,i,k} = \frac{6V b_{90}}{h^3 n_{CA,k}} \frac{t_{0,k}}{t_{net,0}} \frac{\sum_{i=1}^m (a_i^2 b_{0,i})}{\sum_{i=1}^m I_{p,CA,i}} b_{max,i} \quad (32)$$

The derivation of the torsional shear stress presented in [8] and reviewed above, starting with Equation (24), is based on equilibrium considerations of a part of the beam of length equal to the lamination width of the transversal laminations and hence includes the sum of the torsional moments $M_{tor,i}$ and the sum of the polar moments of inertia of the crossing areas $I_{p,CA,i}$.

Expressions for torsional moments and torsional shear stresses of the individual crossing areas can also be derived based on equilibrium considerations of a part of a single longitudinal lamination. Such an alternative and more general derivation is presented below. Definitions and notation according to Figures 13 and 17 are used, where (V, N, M) refer to the forces and the moment acting on the total cross section, (V_i, N_i, M_i) refer to the sum of forces and the moment acting in all k longitudinal laminations for a certain i and $(V_{i,k}, N_{i,k}, M_{i,k})$ refer to the forces and the moment acting in an individual longitudinal lamination i, k . Equilibrium of a part of a single longitudinal lamination i, k gives

$$M_{tor,i,k} = \frac{1}{n_{CA,k}} \frac{t_{0,k}}{t_{net,0}} \left(V_i b_{90} + \Delta V_i \frac{b_{90}}{2} - \Delta M_i \right) \quad (33)$$

where ΔV_i and ΔM_i refer to the changes in force and moment over the length b_{90} .

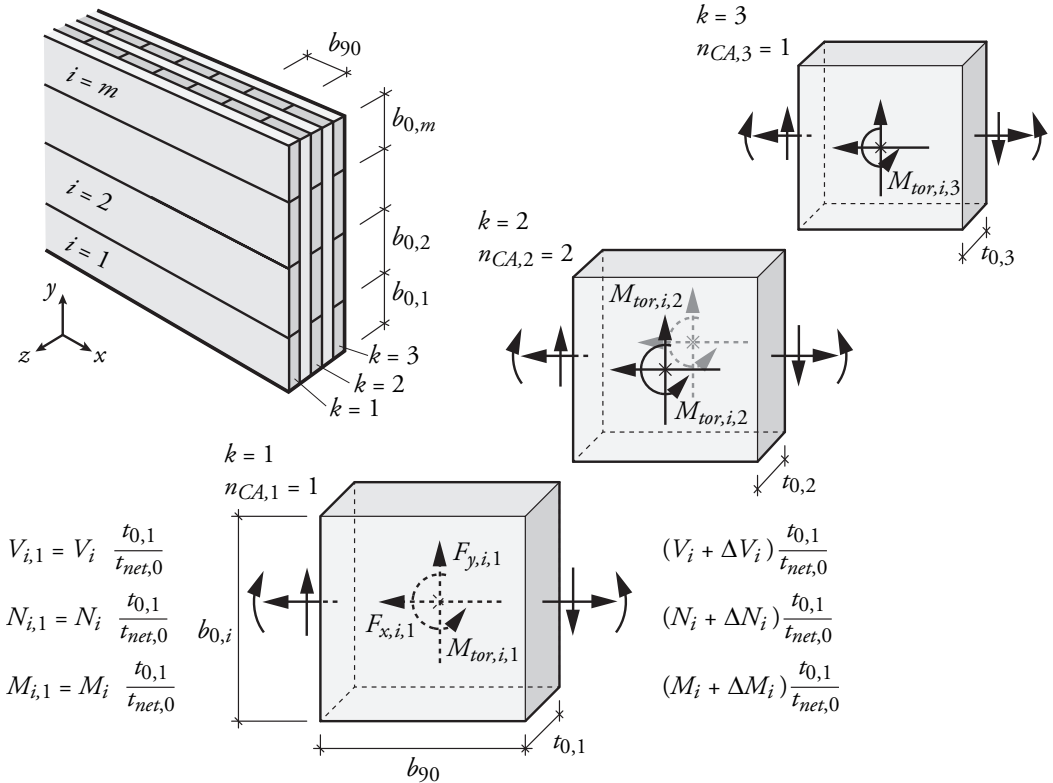


Figure 17: Definition of lamination cross sectional forces and moment $V_{i,k}, N_{i,k}, M_{i,k}$ and the forces and torsional moment $F_{x,i,k}, F_{y,i,k}, M_{tor,i,k}$ acting in the crossing areas.

By assumption of a linear distribution of the normal stress over the beam height h , the bending moment M_i is given by

$$M_i = M \frac{b_{0,i}^3}{h^3} \quad (34)$$

and the axial force N_i is given by

$$N_i = M \frac{12a_i b_{0,i}}{h^3} + N \frac{b_{0,i}}{h} \quad (35)$$

The total shear force V may be assumed to be divided between the longitudinal laminations according to the relation between the lamination width $b_{0,i}$ and the total beam height h , giving

$$V_i = V \frac{b_{0,i}}{h} \quad (36)$$

which corresponds to the shear stress distributions for a location in the beam length direction corresponding to an interface between adjacent transversal laminations, see Figures 11 and 12. Expressing the change in bending moment as $\Delta M = V b_{90}$, assuming $\Delta V = 0$ and using Equations (34) and (36), the torsional moment according to Equation (33) may be express as

$$M_{tor,i,k} = \frac{V b_{90}}{n_{CA,k}} \frac{t_{0,k}}{t_{net,0}} \left(\frac{b_{0,i}}{h} - \frac{b_{0,i}^3}{h^3} \right) \quad (37)$$

Assuming a torsional shear stress distribution as illustrated in Figure 14, corresponding to assuming rigid body rotation of bodies connected by a shear compliant medium, the maximum torsional stress at the middle points of the four sides of the sheared area is

$$\tau_{tor} = \frac{M_{tor}}{I_{p,CA}} \frac{b_{max}}{2} \quad \text{where} \quad I_{p,CA} = \frac{b_0 b_{90}}{12} (b_0^2 + b_{90}^2) \quad (38)$$

where $I_{p,CA}$ is the polar moment of inertia of the rectangular area of side lengths b_0 and b_{90} and where $b_{max} = \max\{b_0, b_{90}\}$. Using Equation (38), the maximum value of the torsional stress at the middle points of the four sides of a crossing area belonging to the longitudinal lamination i, k may be expressed as

$$\tau_{tor,i,k} = \frac{6V}{n_{CA,k}} \frac{t_{0,k}}{t_{net,0}} \frac{b_{max}}{b_{0,i}} \frac{1}{b_{0,i}^2 + b_{90}^2} \left(\frac{b_{0,i}}{h} - \frac{b_{0,i}^3}{h^3} \right) \quad (39)$$

For beams with constant ratio $t_{0,k}/n_{CA,k}$ for all longitudinal layers but with different lamination widths in the transversal and longitudinal layers, i.e. for $b_0 \neq b_{90}$, but still having consistent laminations widths within the transversal and longitudinal layers respectively and hence an integer m number of longitudinal laminations in the beam height direction ($h = mb$), Equation (39) can be simplified to the expression given in Equation (30). For the case of also equal width of the longitudinal and transversal laminations according to $b_0 = b_{90} = b$, Equation (39) can be further simplified to the expression given in Equation (29).

Shear mode III stress interaction criteria

For evaluation of the load bearing capacity with respect to mode III, shear failure in the crossing areas, a stress interaction criterion needs to be chosen since shear stresses in two directions are present. The three shear stress components reviewed above represent either shear stress in the parallel to beam direction (τ_{xz}), shear stress in the perpendicular to beam direction (τ_{yz}) or shear stress in both parallel and perpendicular to beam directions (τ_{tor}) as illustrated in Figure 14. For a single crossing area, bonding a longitudinal and a transversal lamination, these three shear stress components represent for a specific point either longitudinal shear, rolling shear or a combination of both. A shear stress component giving pure longitudinal shear in the longitudinal lamination represents pure rolling shear in the transversal laminations, and vice versa.

A compilation of several possible stress interaction criteria is presented in [8] and evaluated based on a comparison to experimental tests of single crossing areas. All considered stress interaction criteria are based on linear or quadratic interaction of the three stress components τ_{xz} , τ_{yz} and τ_{tor} and comparison to a rolling shear strength f_R (for τ_{xz} and τ_{yz}) and a torsional shear strength $f_{v,tor}$ (for τ_{tor}). Assuming a constant ratio $f_{v,tor}/f_R = 2.33$, the most appropriate failure criteria were found to be

$$\frac{\tau_{tor}}{f_{v,tor}} + \frac{\tau_{xz}}{f_R} \leq 1.0 \quad (40)$$

and

$$\frac{\tau_{tor}}{f_{v,tor}} + \frac{\tau_{yz}}{f_R} \leq 1.0 \quad (41)$$

where stress interaction between τ_{tor} and τ_{xz} according to Equation (40) is referred to as shear failure mode III-A and stress interaction between τ_{tor} and τ_{yz} according to Equation (41) is referred to as shear failure mode III-B. The notation of failure mode III-A and III-B are used in this report, but are not in general used to distinguish between these two different shear failure modes.

The above given failure criteria are based on what can be referred to as *structural properties* of the considered crossing area between two bonded laminations, rather the properties of the material at the material point level.

3.3 Beam with a hole

Compared to a prismatic CLT beam, the stress distribution within a CLT beam with a hole is even more complex. Stress analysis and design recommendations for CLT beams with a hole are treated in [10] and the presented approach is reviewed below. The approach is in general terms based on consideration of the stress distribution in a prismatic beam as presented in Section 3.2 and the use of so called stress concentration factors to account for the differences in stress distribution between a prismatic beam and a beam with a hole. The stress concentration factors are determined based on a large number of FE-analyses considering a variety of beam and hole geometries.

The FE-model used is based on a network of Timoshenko beam elements representing the longitudinal and transversal laminations and spring elements representing the connection between the laminations. The beam elements representing the laminations were assigned a modulus of elasticity of 11 000 MPa and a shear modulus of 690 MPa. The connection between a longitudinal and a transversal lamination was modeled by one spring in the direction parallel to the beam axis, one spring in direction perpendicular to the beam axis and a spring with rotational stiffness about the z -axis. The springs were assigned stiffnesses according to

$$K_x = K_y = K A_{CA} \quad \text{and} \quad K_\varphi = K I_{p,CA} \quad (42)$$

where $A_{CA} = b_0 b_{90}$ is the size of the crossing area, $I_{p,CA}$ is the polar moment of inertia of the crossing area and where the so called slip modulus was assigned as $K = 7.5 \text{ N/mm}^3$.

A parameter study based on FE-analysis was performed, considering different beam heights and hole sizes and aspect ratios. All analyses were performed considering equal width of the longitudinal and transversal laminations according to $b_0 = b_{90} = b = 150 \text{ mm}$. The ratio between the total width of the transversal layers and the gross cross section width was consistently $t_{net,90}/t_{gross} = 0.20$ and the ratio between the gross cross section width and the number of crossing areas in the beam width direction was consistently $t_{gross}/n_{CA} = 50 \text{ mm}$.

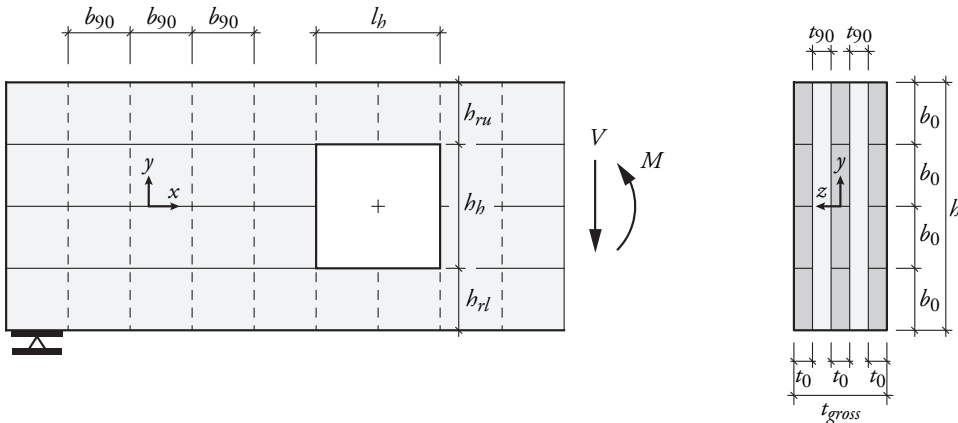


Figure 18: CLT beam with a hole, definitions of geometry parameters.

The beam height was varied in the range $600 \leq h \leq 1800$ mm. The hole dimensions were varied in the range $b \leq l_h \leq h$ and $b \leq h_h \leq 0.5h$ while hole aspects ratios in the range $1 \leq l_h/h_h \leq 4$ were considered. The beam and hole geometries were consistently based on integer multiples of the lamination width $b = 150$ mm and the beam and hole edges always coincided with the lamination edges.

It appears as if only holes placed centrally with respect to the beam height (y) direction were considered in the parameter study presented in [10].

3.3.1 Bending

For a beam with a hole, the maximum normal stress due to bending may appear at the hole or at a location in the beam where the cross section is complete but where the bending moment has its maximum value. Calculation of maximum bending stress for a complete cross section, without a hole, is treated in Section 3.2. At a hole, the maximum normal stress may be calculated as the sum of the stress from bending of the full cross section considering complete interaction between the upper and lower parts of the beam and a contribution from the additional local bending of the upper or lower part, respectively. For a beam with a rectangular hole of length l_h and height h_h , centrally placed with respect to the beam height (y) direction, the normal stress at the hole center due to bending of the full cross section is given by

$$\sigma_{x,M} = \frac{M_h}{W_h} \quad \text{with} \quad W_h = \frac{t_{net,0} (h^3 - h_h^3)}{6h} \quad (43)$$

where M_h is the bending moment at the center of the hole, $t_{net,0} = \sum t_{0,i}$ is the net cross section width considering the longitudinal layers only and h is the beam height. The normal stress due to the additional bending of the beam parts above and below the hole may be expressed as

$$\sigma_{x,V} = \frac{M_r}{W_r} \quad \text{with} \quad W_r = \frac{t_{net,0} (h - h_h)^2}{24} \quad (44)$$

where $M_r = V/2 \cdot l_h/2$ is the additional bending moment in the upper and lower part of the beam, respectively. The maximum normal stress in the beam length direction due to bending is then given by

$$\sigma_{x,h} = \sigma_{x,M} + \sigma_{x,V} = \frac{6M_h h}{t_{net,0} (h^3 - h_h^3)} + \frac{6V l_h}{t_{net,0} (h - h_h)^2} \quad (45)$$

The contribution from additional local bending of the beam parts above and below the hole is for beams with circular holes commonly disregarded.

3.3.2 Tension perpendicular to beam axis

Introducing a hole in a beam also means introducing perpendicular to beam axis tensile and compressive forces. The perpendicular to beam axis tensile force is in [10] calculated based on the approach given in the German National Annex to Eurocode 5 [2] for conventional timber or glulam beams with a hole. The tensile force perpendicular to the beam axis $F_{t,90,h}$, composed of a contribution from the shear force $F_{t,90,V}$ and a contribution from the bending moment $F_{t,90,M}$, is then given by

$$F_{t,90,h} = F_{t,90,V} + F_{t,90,M} \quad (46)$$

where

$$F_{t,90,V} = \frac{V h_h}{4h} \left(3 - \frac{h_h^2}{h^2} \right) \quad (47)$$

$$F_{t,90,M} = \frac{0.008M}{h_r} \quad (48)$$

and where M and V refer to the bending moment and shear force at the edge of the hole and where $h_r = \min\{h_{ru}, h_{rl}\}$. The perpendicular to beam axis tensile force $F_{t,90,h}$ according to Equation (46) is in [10] stated as being slightly larger but in general in good agreement with the results of the FE-analyses of CLT beams with a hole. The perpendicular to beam axis tensile stress in the transversal laminations at the edge of the hole, giving parallel to grain tensile stress in the transversal laminations, may then be calculated according to

$$\sigma_{t,0,h} = \frac{F_{t,90,h}}{a_r t_{net,90}} k_k \quad \text{with} \quad a_r = \min\{b_{90}, 0.3(h + h_h)\} \quad (49)$$

where $k_k = 2.0$ and $t_{net,90}$ is the beam net cross section width considering the transversal layers.

3.3.3 Shear mode I

For shear mode I, corresponding to the gross shear failure mode, the maximum shear stress for a beam with a hole may, according to [10], be expressed as

$$\tau_{xy,gross,h} = \frac{3}{2} \frac{V}{t_{gross} (h - h_h)} \quad (50)$$

without any adjustment due to stress concentrations induced by the hole.

3.3.4 Shear mode II

For shear mode II, corresponding to the net shear failure mode, the maximum shear stress for a beam with a hole may, according to [10], be expressed as

$$\tau_{xy,net,h} = \frac{3}{2} \frac{V}{t_{net}h} k_{h,2} k_b \quad \text{with} \quad k_{h,2} = 0.103 \frac{h_h l_h}{h^2} m^2 + 1.27 \quad (51)$$

where t_{net} refers to either $t_{net,0}$ or $t_{net,90}$, with the smaller of the two being decisive for the maximum stress value. For longitudinal and transversal lamination widths in the range $100 \leq b \leq 200$ mm is $k_b = (b/150)^{1/3}$, with b in mm.

3.3.5 Shear mode III

Shear mode III, corresponding to failure in a crossing area, involves shear stress components τ_{xz} and τ_{yz} . The shear stresses acting in the crossings areas may, according to the composite beam model described in Section 3.2, be considered to be composed of three separate contributions; shear stress parallel to the beam axis τ_{xz} , shear stress perpendicular to the beam axis τ_{yz} and torsional shear stress τ_{tor} . The respective maximum shear stress values in the vicinity of a hole as stated in [10] are reviewed below, considering a beam composed of longitudinal and transversal laminations of equal width according to $b_0 = b_{90} = b$.

At a hole, the maximum shear stress parallel to the beam axis may be expressed as

$$\tau_{xz,h} = \frac{6V}{b^2 n_{CA}} \left(\frac{1}{m^2} - \frac{1}{m^3} \right) k_{h,2} k_b \quad \text{with} \quad k_{h,2} = 0.103 \frac{h_h l_h}{h^2} m^2 + 1.27 \quad (52)$$

where n_{CA} is the number of crossing areas in the beam width direction and m is the number of longitudinal laminations in the beam height direction. For lamination widths in the range $100 \leq b \leq 200$ mm is $k_b = (b/150)^{1/3}$, with b in mm.

At a hole, the maximum shear stress perpendicular to the beam axis may be expressed as

$$\tau_{yz,h} = \frac{F_{t,90,h}}{a_r h_r n_{CA}} \quad \text{with} \quad a_r = \min \{b_{90}, 0.3(h + h_h)\} \quad (53)$$

where $F_{t,90,h}$ is the perpendicular to beam axis tensile stress according to Equation (46) and where $h_r = \min\{h_{ru}, h_{rl}\}$.

At a hole, the maximum torsional shear stress may be expressed as

$$\tau_{tor,h} = \frac{3V}{b^2 n_{CA}} \left(\frac{1}{m} - \frac{1}{m^3} \right) k_{h,1} k_b \quad \text{with} \quad k_{h,1} = 1.81 \frac{l_h}{h} \frac{h_h}{h - h_h} + 1.14 \quad (54)$$

where n_{CA} is the total number of crossing areas in the beam width direction and m is the number of longitudinal laminations in the beam height direction. For lamination widths in the range $100 \leq b \leq 200$ mm is $k_b = (b/150)^{1/3}$, with b in mm.

3.4 Beam with an end-notch

As for the case of a beam with a hole, stress analysis and design recommendations for a beam with an end-notch is presented in [10]. The approach is also for this case, in general terms, based on consideration of the stress distribution in a prismatic beam as presented in Section 3.2 and the use of so called stress concentration factors to account for the differences in stress distribution between a prismatic beam and an end-notched beam. The stress concentration factors are determined based on a large number of FE-analyses considering a variety of beam and notch geometries.

The same type of FE-model, composed of Timoshenko beam elements as representation of the longitudinal and transversal laminations and spring elements as representation of the bonding between laminations as described in Section 3.3, was used for a parameters study comprising different beam heights and notch sizes and aspect ratios. All analyses were performed considering equal width of the longitudinal and transversal laminations according to $b_0 = b_{90} = b = 150$ mm. The ratio between the total width of the transversal layers and the gross cross section width was consistently $t_{net,90}/t_{gross} = 0.20$ and the ratio between the gross cross section width and the number of crossing areas in the beam width direction was consistently $t_{gross}/n_{CA} = 50$ mm. The beam height was varied in the range $300 \leq h \leq 1200$ mm. The notch depth was varied in the range $b \leq (h - h_{ef}) \leq 0.5h$ and the distance between the support and the notch corner was varied in the range $b \leq c \leq 0.5h$. The ratio between the distance from the support to the notch corner and the effective beam height was for all considered analyses $c/h_{ef} \leq 1.0$. The beam and notch geometries were consistently based on integer multiples of the lamination width $b = 150$ mm and the beam and notch edges always coincided with the lamination edges.

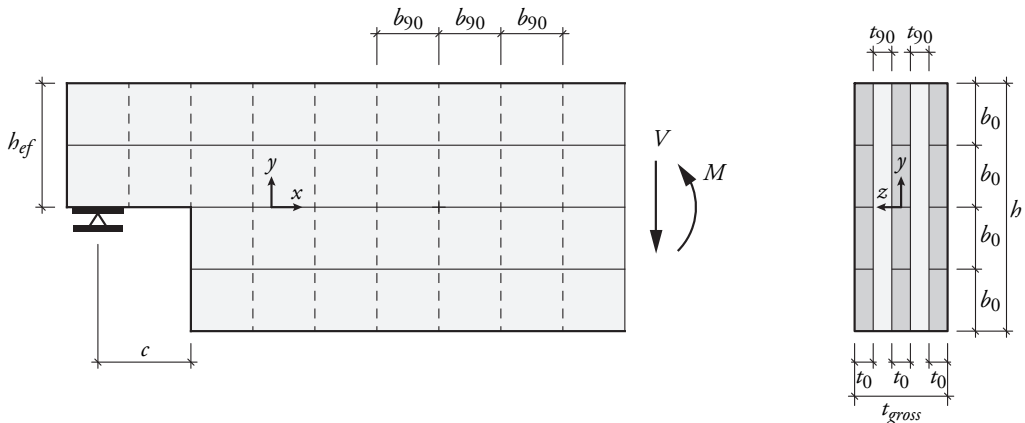


Figure 19: CLT beam with an end-notch, definitions of geometry parameters.

3.4.1 Bending

For a beam with an end-notch, the maximum normal stress due to bending may appear at the reduced cross section at the notch or at a location in the beam where the cross section is complete but where the bending moment has its maximum value. Calculation of maximum normal stress for a complete cross section, without an end-notch, is treated in Section 3.2. At the notch corner, the normal stress due to bending may be calculated as

$$\sigma_{x,n} = \frac{Vc}{W_n} \quad \text{with} \quad W_n = \frac{t_{net,0}h_{ef}^2}{6} \quad (55)$$

where V is the shear force (or the support reaction force), $t_{net,0} = \sum t_{0,i}$ is the net cross section width considering the longitudinal layers only and where c and h_{ef} are defined in Figure 19.

3.4.2 Tension perpendicular to beam axis

For a beam with loading and geometry according to Figure 19, tensile stress perpendicular to the beam axis is introduced at the notch corner. Perpendicular to beam axis tensile force is in [10] calculated based on the approach presented in the German National Annex to Eurocode 5 [2] for conventional timber or glulam beams having an end-notch. The tensile force perpendicular to the beam axis $F_{t,90,n}$ is then given by

$$F_{t,90,n} = 1.3V \left(3 \left(1 - \frac{h_{ef}}{h} \right)^2 - 2 \left(1 - \frac{h_{ef}}{h} \right)^3 \right) \quad (56)$$

where V is the shear force (or the support reaction force) and h_{ef} is the effective beam height at the notch. The perpendicular to beam axis tensile force $F_{t,90,n}$ according to Equation (56) is in [10] stated as being slightly larger compared to forces found from the FE-analyses of beams with an end-notch. The perpendicular to beam axis tensile stress in the transversal laminations at the notch, giving parallel to grain tensile stress in the transversal laminations, may be calculated according to

$$\sigma_{t,0,n} = \frac{F_{t,90,n}}{l_r t_{net,90}} k_k \quad \text{with} \quad l_r = \min \{ b_{90}, 0.5(h - h_{ef}) \} \quad (57)$$

where $k_k = 2.0$ and $t_{net,90}$ is the net cross section width considering the transversal layers.

3.4.3 Shear mode I

For shear mode I, corresponding to the gross shear failure mode, may according to [10] the maximum shear stress for a beam with an end-notch be expressed as

$$\tau_{xy,gross,n} = \frac{3}{2} \frac{V}{t_{gross} h_{ef}} \quad (58)$$

without any adjustment due to stress concentrations induced by the notch.

3.4.4 Shear mode II

For shear mode II, corresponding to the net shear failure mode, may according to [10] the maximum shear stress for a beam with an end-notch be expressed as

$$\tau_{xy,net,n} = \frac{3}{2} \frac{V}{t_{net}h} k_n k_b \quad \text{with} \quad k_n = 0.877 \left(\frac{h_{ef}}{h} \right)^{k_c} \quad \text{and} \quad k_c = -1.81 \left(\frac{c}{h} \right)^{0.479} \quad (59)$$

and where $t_{net} = \min \{t_{net,0}, t_{net,90}\}$. For longitudinal and transversal lamination widths in the range $100 \leq b \leq 200$ mm is $k_b = (b/150)^{1/3}$, with b in mm.

3.4.5 Shear mode III

Shear mode III, corresponding to failure in a crossing area, involves shear stress components τ_{xz} and τ_{yz} . The shear stresses acting in the crossings areas may, according to the composite beam model described in Section 3.2, be considered to be composed of three separate contributions; shear stress parallel to the beam axis τ_{xz} , shear stress perpendicular to the beam axis τ_{yz} and torsional shear stress τ_{tor} . According to [10], the shear stress parallel to the beam axis τ_{xz} was from the FE-analyses found to be lower than the shear stress perpendicular to the beam axis τ_{yz} . Hence, only shear stress components τ_{tor} and τ_{yz} were considered for evaluation. The respective maximum shear stress values in the vicinity of a notch as stated in [10] are reviewed below, considering a beam composed of longitudinal and transversal laminations of equal width according to $b_0 = b_{90} = b$.

At a notch, the maximum shear stress perpendicular to the beam axis may be expressed as

$$\tau_{yz,n} = \frac{F_{t,90,n}}{l_r h_n n_{CA}} \quad \text{with} \quad h_n = \min \{h_{ef}, h - h_{ef}\} \quad (60)$$

and where $F_{t,90,n}$ is the perpendicular to beam axis tensile force according to Equation (56) and where $l_r = \min \{b_{90}, 0.5(h - h_{ef})\}$.

At a notch, the maximum torsional shear stress may be expressed as

$$\tau_{tor,n} = \frac{3V}{b^2 n_{CA}} \left(\frac{1}{m} - \frac{1}{m^3} \right) k_n k_b \quad \text{with} \quad k_n = 0.877 \left(\frac{h_{ef}}{h} \right)^{k_c} \quad \text{and} \quad k_c = -1.81 \left(\frac{c}{h} \right)^{0.479} \quad (61)$$

and where n_{CA} is the number of crossing areas in the beam width direction and m is the number of laminations in the beam height direction in the longitudinal layers. For lamination widths in the range $100 \leq b \leq 200$ mm is $k_b = (b/150)^{1/3}$, with b in mm.

3.5 Stiffness

3.5.1 Bending stiffness

For simplified calculations of strength and stiffness of CLT elements at in-plane beam loading, normal stresses in the plane of the element is commonly assumed to be carried only by the layers that are oriented with the grain direction parallel to the stress direction. This assumption is motivated by the large difference in stiffness between parallel and perpendicular to grain loading directions, with $E_0/E_{90} \approx 15 - 35$. The normal stress parallel to the beam axis is furthermore commonly assumed to have a linear (and continuous) distribution over the entire beam height, see Figure 20, and the bending stiffness D_{EI} can then be expressed as

$$D_{EI} = E_0 I \quad \text{where} \quad I = I_{net} = \frac{t_{net,0} h^3}{12} \quad (62)$$

where $t_{net,0} = \sum t_{0,i}$ is the net cross section width considering the longitudinal layers only. The linear and continuous normal stress distribution corresponds to conventional beam theory assumption that a plane cross sections remains plane during deformation.

Sliding between the longitudinal laminations may occur for elements without edge-bonding, especially if there are gaps between the laminations. In this situation, the normal stress distribution will be discontinuous, see Figure 20, and the bending stiffness will for this situation be lower than suggested according to Equation (62).

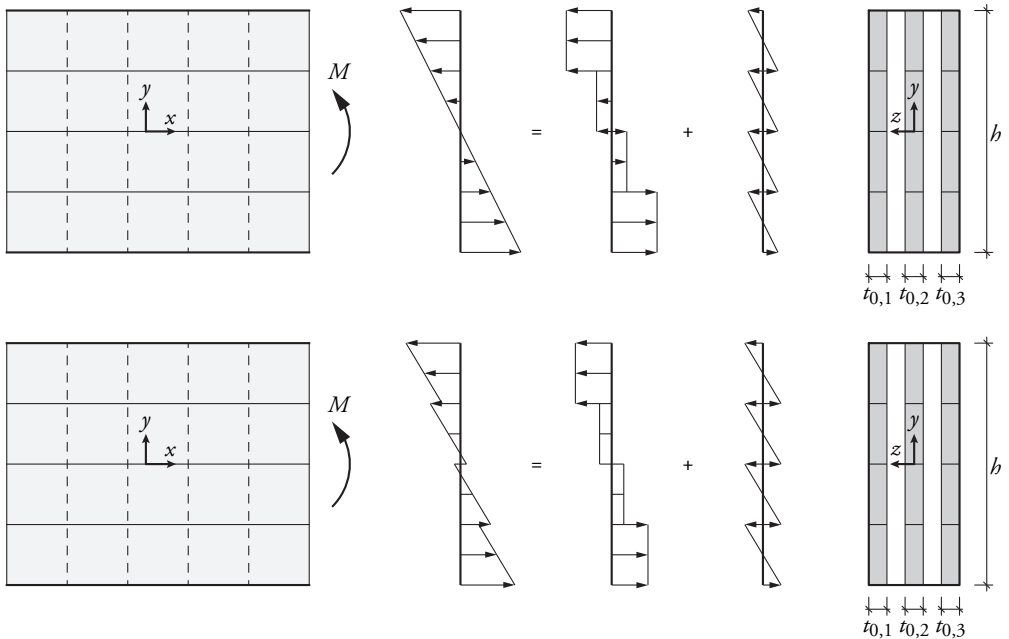


Figure 20: Continuous (top) and discontinuous stress distribution (bottom).

3.5.2 Shear stiffness

The shear stiffness of a CLT beam with edge-bonding (narrow-face bonding) can in general be expected to be equal to that of a beam of the same dimensions but with homogeneous orientation of all laminations. The shear stiffness of a CLT beam without narrow-face bonding can however in general be expected to be lower compared to that of a homogeneous beam, due to discontinuities at the unbonded faces and hence the occurrence of traction-free surfaces at the areas where narrow faces of adjacent laminations of the same layer meet.

A model to account for the additional shear deformations due to relative sliding and rotation of center-lines of the longitudinal laminations with respect to the transversal laminations for CLT beams without edge-bonding is presented in [8], [9] and [11]. In addition to the shear straining of the the individual laminations in the xy -plane, additional shear strains γ_{xy} and γ_{tor} according to Figure 21 are considered.

The shear compliance due to relative sliding and rotation is assumed to be governed by the so called slip modulus of the crossing areas K [N/mm³]. The relative sliding and rotations are assumed to be dominated by rolling shear straining in the immediate vicinity of the bonded crossing area and the value of K is hence assumed to be independent of the lamination thicknesses t_0 and t_{90} . The model is based on assumptions of equal widths of the longitudinal and transversal laminations according to $b_0 = b_{90} = b$. It is furthermore implicitly assumed that the ratio $t_{0,k}/n_{CA,k}$ is constant for all longitudinal layers, giving equal loading situation in terms of shear stresses for all crossing areas in the beam width direction. The relative sliding and the relative rotation over a crossing area between a longitudinal and a transversal lamination is considered by a conventional spring and a rotational spring respectively, with spring stiffnesses according to

$$K_x = K A_{CA} \quad \text{and} \quad K_\varphi = K I_{p,CA} \quad (63)$$

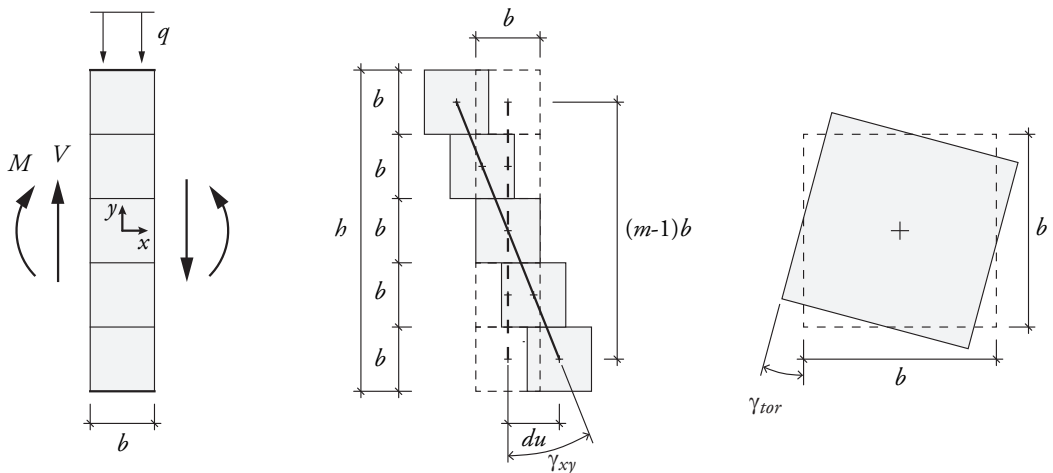


Figure 21: Definition of shear strain components γ_{xy} and γ_{tor} .

where $A_{CA} = b^2$ is the size of the crossing area and $I_{p,CA} = b^4/6$ is the polar moment of inertia of the crossing area. The shear strain components defined in Figure 21 may then be expressed as

$$\gamma_{xy} = \frac{2du}{b(m-1)} = \frac{2\tau_{xz}}{Kb(m-1)} \quad (64)$$

and

$$\gamma_{tor} = \frac{M_{tor}}{KI_{p,CA}} = \frac{2\tau_{tor}}{Kb} \quad (65)$$

where m is the number of longitudinal laminations in the beam height direction, i.e. $h = mb$. The shear stress components τ_{xy} and τ_{tor} are the parallel to beam axis shear stress and the torsional shear stress, respectively, caused by the shear force V acting on the complete cross section and discussed in Section 3.2.3 above. Using the relations between the shear force V and the stress components τ_{xz} and τ_{tor} according to Equations (19) and (29), respectively, the shear strain components may be expressed as

$$\gamma_{xy} = \frac{12V}{b^3K} \frac{1}{m^3} \frac{1}{n_{CA}} \quad (66)$$

and

$$\gamma_{tor} = \frac{6V}{b^3K} \left(\frac{1}{m} - \frac{1}{m^3} \right) \frac{1}{n_{CA}} \quad (67)$$

where n_{CA} is the number of crossing areas in the beam width direction. The total shear strain γ_{CA} due to relative sliding and relative rotation over the crossing areas can then be expressed as the sum of the two components according to

$$\gamma_{CA} = \gamma_{xy} + \gamma_{tor} \quad (68)$$

An effective shear modulus $G_{ef,CA}$ accounting for relative sliding and rotation over the crossing areas and representing a CLT beam gross cross section may then be defined according to

$$G_{ef,CA} = \frac{V}{k_s A_{gross} \gamma_{CA}} = \frac{Kb^2}{5} \frac{n_{CA}}{t_{gross}} \frac{m^2}{m^2 + 1} \quad (69)$$

using a value of the shear correction factor according to $k_s = 5/6$.

The total effective shear modulus for a CLT gross cross section, accounting for both within lamination shear strains in the xy -plane and for relative sliding and rotation of crossing areas, may finally be expressed as

$$G_{ef,CLT} = \left(\frac{1}{G_{lam}} + \frac{1}{G_{ef,CA}} \right)^{-1} \quad (70)$$

where G_{lam} is the shear modulus of the laminations for longitudinal shear loading.

4 RESULTS

Results regarding beam strength and stiffness are presented below for the tests described in Section 2. Results regarding beam strength are presented in Section 4.1 while results regarding beam stiffness are presented in Sections 4.2 and 4.3. Results are presented both in terms of totally applied loads and also in terms of stress components at maximum load, based on the analytical models for stress analysis presented in Section 3.

The reported loads do for test series A, B and C include an additional load of 3 kN compared to the loads recorded by the load cell during testing, in order to account for the self-weight of the steel beam and the steel plates used at the load introduction points for these test series.

4.1 Beam strength

A summary of the test results in terms of failure loads (maximum applied total load) is presented in Table 3. More detailed results in terms of stress components at maximum load, graphs of load vs. deflection and photos from the failed specimens are given below for the five different test series.

Table 3: Summary of failure loads (maximum applied loads) for the five test series.

	Test series A	Test series B	Test series C	Test series D	Test series E
	F_{max} [kN]	F_{max} [kN]	F_{max} [kN]	F_{max} [kN]	F_{max} [kN]
test #1	277.1	523.9	413.2	350.9	491.3
test #2	295.0	475.6	363.2	349.3	519.5
test #3	293.5	491.9	335.6	361.6	513.0
test #4	304.3	502.0	412.9	345.5	476.3
mean	292.5	498.3	381.2	351.8	500.0
std	11.3	20.2	38.4	6.90	19.9
cov	3.9 %	4.1 %	10.1 %	2.0 %	4.0 %

Test series A

The results for test series A, in terms of maximum values of stress components at maximum load, are given in Table 4. Equations used for calculation of stresses are indicated in the table. These stress values are based on the assumption of equal widths of the laminations of the longitudinal and transversal layers according to $b_0 = b_{90} = 150$ mm and of constant ratio $t_{0,k}/n_{CA,k}$ for all longitudinal layers. A nominal beam height $h = 600$ mm and hole height and length according to $h_h = 300$ mm and $l_h = 300$ mm, respectively, are further assumed. For calculation of stress components $\sigma_{t,0,h}$ and $\tau_{yz,h}$ in Table 4 is the width of the first transversal laminations next to the hole assumed to be equal to the full width of the transversal laminations, i.e. $b_{90} = 150$ mm. The stress components corresponding to the the assumed dominating mode of failure are indicated by being underlined.

Graphs of applied load vs. global beam deflection are shown in Figure 22 for the individual tests, with beam deflection being measured at midspan at the bottom side of the beam as illustrated in Figure 8. Missing data points for test A4 at load levels of approximately 260 kN are due to problems with the potentiometer measuring the global beam deflection. Photos from the tests are shown in Figure 23.

The failure modes for test A1 and A4 are categorized as failure due to bending at the hole, while tests A2 and A3 are categorized as bending failures occurring between the two load introduction points. For tests A1, the global failure appears to have been initiated by a bending/tension failure in one of the bottom-most longitudinal laminations at a location between the hole and the support. For tests A2 and A3, the global failures appear to have been initiated around knots and at finger joints, respectively, located in the lower-most laminations at locations between the two load introduction points. For test A4, the global failure appears to have been initiated by a bending/tension failure at a finger joint in one of the external lower-most lamination below the hole and at a finger joint in the other external lower-most lamination at a location between the hole and the closest load introduction point.

Table 4: Failure load (maximum load) and corresponding stress values for test series A.

	F_{max}	σ_x	$\sigma_{x,h}$	$\sigma_{t,0,h}$	$\tau_{xy,gross,h}$	$\tau_{xy,net,h}$	$\tau_{xz,h}$	$\tau_{yz,h}$	$\tau_{tor,h}$
	(4)	(45)	(49)	(50)	(51)	(52)	(53)	(54)	
	[kN]	[MPa]	[MPa]	[MPa]	[MPa]	[MPa]	[MPa]	[MPa]	[MPa]
A1	277.1	34.6	<u>42.9</u>	18.5	4.33	14.6	0.73	0.62	2.21
A2	295.0	<u>36.9</u>	45.6	19.7	4.61	15.5	0.78	0.66	2.36
A3	293.5	<u>36.7</u>	45.4	19.6	4.59	15.4	0.77	0.65	2.34
A4	304.3	38.0	<u>47.1</u>	20.3	4.76	16.0	0.80	0.68	2.43
mean	292.5	36.6	45.3	19.5	4.57	15.4	0.77	0.65	2.34

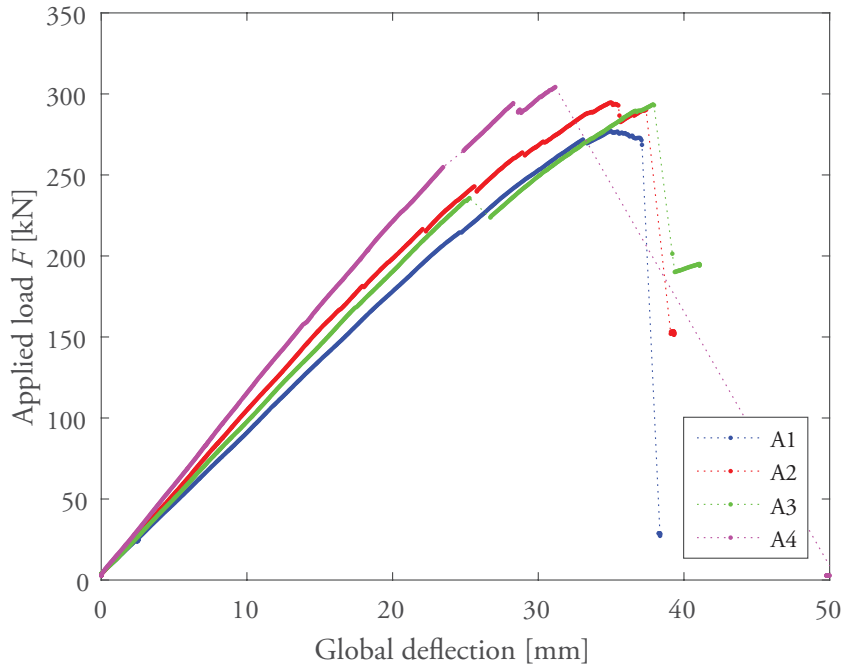


Figure 22: Applied load F vs. global deflection for test series A.

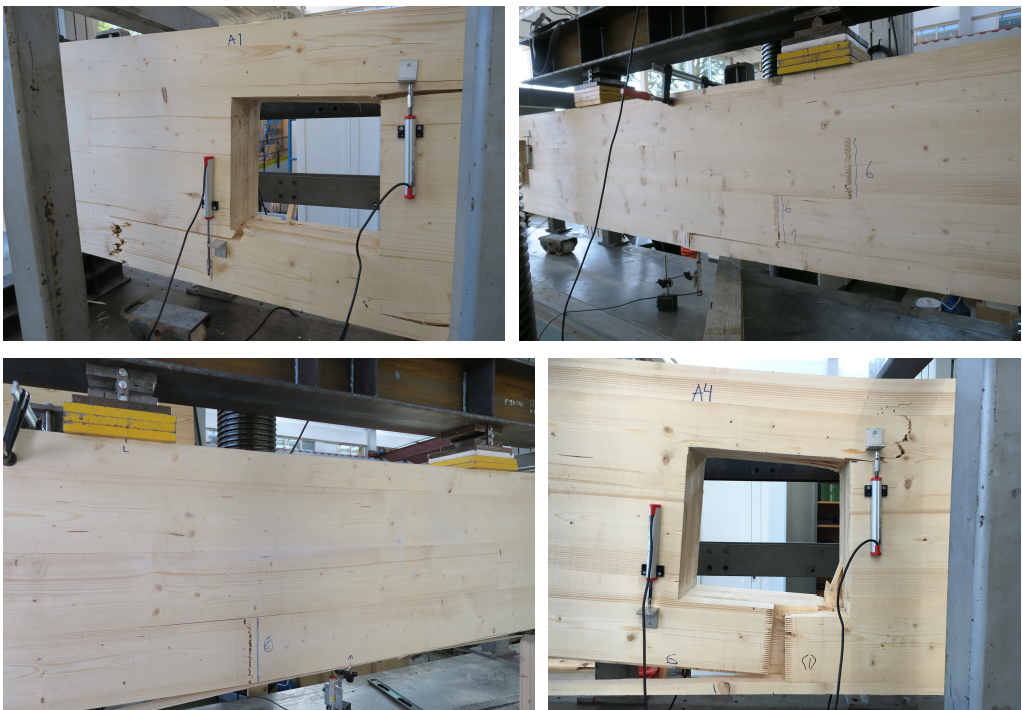


Figure 23: A1 (top left), A2 (top right), A3 (bottom left) and A4 (bottom right).

Test series B

The results for test series B, in terms of maximum values of stress components at maximum load, are given in Table 5. Equations used for calculation of stresses are indicated in the table. These stress values are based on the assumption of equal widths of the laminations of the longitudinal and transversal layers according to $b_0 = b_{90} = 150$ mm and of constant ratio $t_{0,k}/n_{CA,k}$ for all longitudinal layers. A nominal beam height $h = 600$ mm and hole height and length according to $h_h = 300$ mm and $l_h = 300$ mm, respectively, are further assumed. For calculation of stress components $\sigma_{t,0,h}$ and $\tau_{yz,h}$ in Table 5 is the width of the first transversal laminations next to the hole assumed to be equal to the full width of the transversal laminations, i.e. $b_{90} = 150$ mm. The stress components corresponding to the the assumed dominating mode of failure are indicated by being underlined.

Graphs of applied load vs. global beam deflection are shown in Figure 24 for the individual tests, with beam deflection being measured at the bottom side of the beam at one of the load introduction points as illustrated in Figure 8. Photos from the tests are shown in Figure 25.

The mode of failure was very similar for all four individual tests of test series B. The global failure appears for all test to have been initiated by shear stress in the crossing area as interaction of torsional shear stress τ_{tor} and perpendicular to beam axis shear stress τ_{yz} , see Equation (41), which in this report is referred to as shear failure mode III-B. At maximum load, cracks in general appeared simultaneously at the two corners of the hole exposed to perpendicular to beam axis tensile stress. Cracks in the parallel to grain direction in both the longitudinal and transversal laminations also appeared at these locations, indicating shear mode I (gross shear) failure which is believed to be a secondary failure following after the initial shear failure in mode III-B.

Table 5: Failure load (maximum load) and corresponding stress values for test series B.

	F_{max}	σ_x	$\sigma_{x,h}$	$\sigma_{t,0,h}$	$\tau_{xy,gross,h}$	$\tau_{xy,net,h}$	$\tau_{xz,h}$	$\tau_{yz,h}$	$\tau_{tor,h}$
	(4)	(45)	(49)	(50)	(51)	(52)	(53)	(54)	
	[kN]	[MPa]	[MPa]	[MPa]	[MPa]	[MPa]	[MPa]	[MPa]	
B1	523.9	18.2	29.1	20.5	5.46	18.4	0.92	<u>0.68</u>	<u>2.79</u>
B2	475.6	16.5	26.4	18.6	4.95	16.7	0.83	<u>0.62</u>	<u>2.53</u>
B3	491.9	17.1	27.3	19.2	5.12	17.2	0.86	<u>0.64</u>	<u>2.62</u>
B4	502.0	17.4	27.9	19.6	5.23	17.6	0.88	<u>0.65</u>	<u>2.67</u>
mean	498.3	17.3	27.7	19.5	5.19	17.5	0.87	0.65	2.65

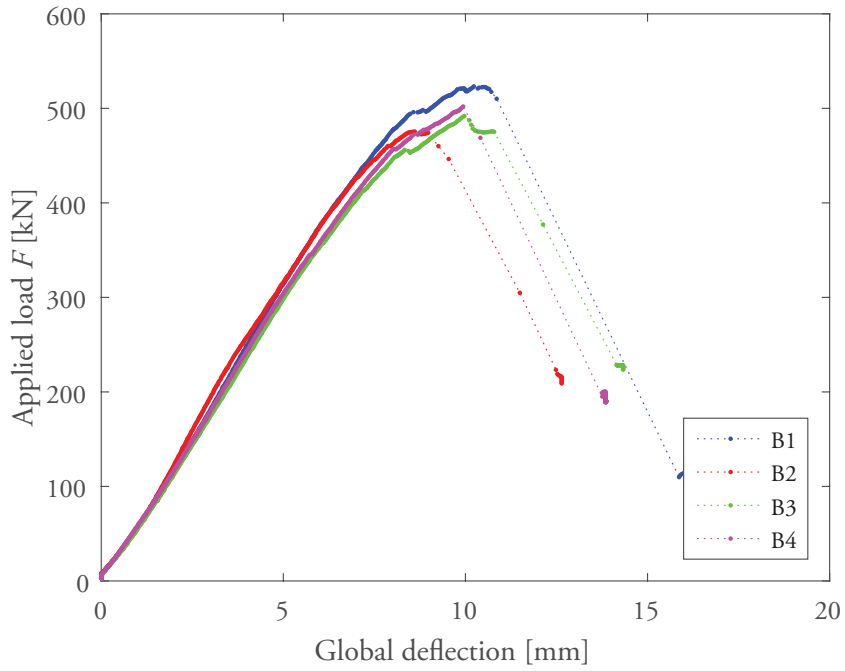


Figure 24: Applied load F vs. global deflection for test series B.



Figure 25: B1 (top left), B2 (top right), B3 (bottom left) and B4 (bottom right).

Test series C

The results for test series C, in terms of maximum values of stress components at maximum load, are given in Table 6. Equations used for calculation of stresses are indicated in the table. These stress values are based on the assumption of equal widths of the laminations of the longitudinal and transversal layers according to $b_0 = b_{90} = 150$ mm and of constant ratio $t_{0,k}/n_{CA,k}$ for all longitudinal layers. A nominal beam height $h = 600$ mm is further assumed. The stress components corresponding to the the assumed dominating mode of failure are indicated by being underlined.

Graphs of applied load vs. global beam deflection are shown in Figure 26 for the individual tests, with beam deflection being measured at the bottom side of the beam at beam mid-span as illustrated in Figure 8. Photos from the tests are shown in Figure 27.

Results in terms of parallel to beam axis shear stress τ_{xz} and torsional shear stress τ_{tor} are also given in Table 7, with stress values based on the actual geometry of the specimens in terms of longitudinal and transversal lamination widths b_0 and b_{90} and ratio $t_{0,k}/n_{CA,k}$ according to Figure 6. An additional (fictitious) reference beam geometry, C-ref, is also included with stress values based on the mean value of the failure load for the four actual tests. The reference geometry is based on assumed lamination widths as $b_0 = b_{90} = 150$ mm. The ratio $t_{0,k}/n_{CA,k}$ is however according to the actual specimens.

The mode of failure is for all four individual tests categorized as bending failure. For test C1, the global failure appears to have been initiated at knots in the lower-most longitudinal laminations. At maximum load, sudden crack propagation in the lower-most lamination took place and cracks also appeared in the second and third lower-most external laminations. For test C2, the global failure appears to have been initiated at a finger joint in one of the external lower-most longitudinal laminations at a location (in the beam length direction) close to one of the load introduction points. It appears as the global failure also for tests C3 and C4 was initiated at finger joints in the lower-most longitudinal laminations in the area of maximum bending moment, between the load introduction points.

Table 6: Failure load (maximum load) and corresponding stress values for test series C.

	F_{max}	σ_x	$\tau_{xy,gross}$	$\tau_{xy,0}$	$\tau_{xy,90}$	τ_{xz}	τ_{yz}	τ_{tor}
	[kN]	(4) [MPa]	(12) [MPa]	(13) [MPa]	(14) [MPa]	(19) [MPa]	(23) [MPa]	(29) [MPa]
C1	413.2	<u>43.0</u>	3.23	4.30	12.9	0.65	0.37	1.61
C2	363.2	<u>37.8</u>	2.84	3.78	11.3	0.57	0.33	1.42
C3	335.6	<u>35.0</u>	2.62	3.50	10.5	0.52	0.30	1.31
C4	412.9	<u>43.0</u>	3.23	4.30	12.9	0.65	0.37	1.61
mean	381.2	39.7	2.98	3.97	11.9	0.60	0.35	1.49

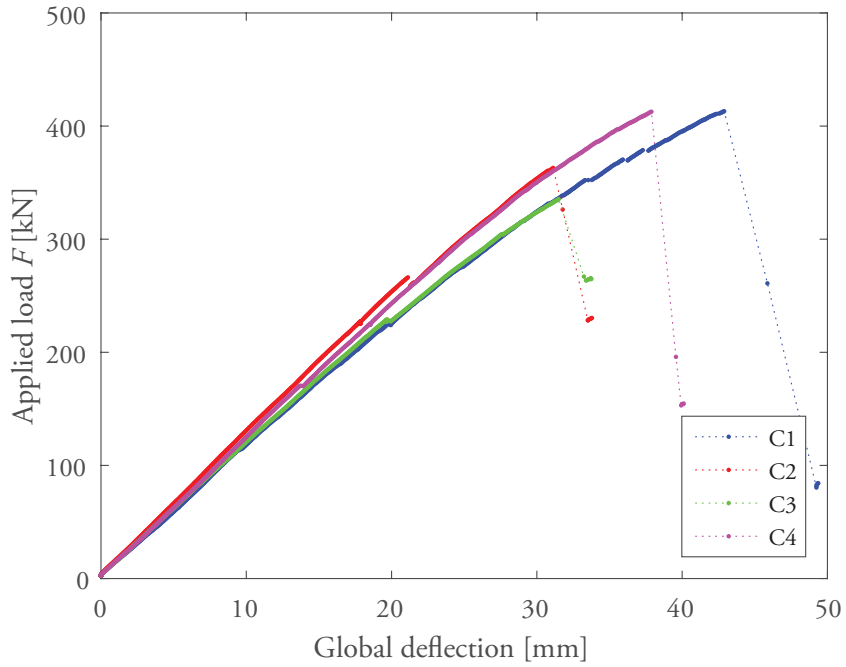


Figure 26: Applied load F vs. global deflection for test series C.



Figure 27: C1 (top left), C2 (top right), C3 (bottom left) and C4 (bottom right).

Table 7: Shear stresses τ_{xz} and τ_{tor} based on actual specimen geometries, test series C.

Specimen	V_{max} [kN]	b_{90} [mm]	i [-]	$b_{0,i}$ [mm]	$\tau_{xz,i,1}$	$\tau_{tor,i,1}$	$\tau_{tor,i,1}$
					[MPa] Eq. (17)	[MPa] Eq. (32)	[MPa] Eq. (39)
C1	206.6	146	4	124	0.91	2.07	2.62
			3	172	0.34	2.44	2.14
			2	172	0.31	2.44	2.14
			1	132	0.90	2.07	2.47
C2	181.6	146	4	85	0.86	1.71	3.03
			3	172	0.43	2.02	1.87
			2	172	0.14	2.02	1.87
			1	172	0.72	2.02	1.87
C3	167.8	146	4	154	0.69	1.74	1.79
			3	172	0.19	1.94	1.73
			2	172	0.35	1.94	1.73
			1	102	0.77	1.65	2.50
C4	206.5	146	5	30	1.07	1.97	4.47
			4	172	0.70	2.33	2.12
			3	172	0.05	2.33	2.12
			2	172	0.59	2.33	2.12
			1	59	1.02	1.97	3.98
<i>C-ref</i>	190.6	150	4	150	0.79	1.99	1.99
			3	150	0.26	1.99	1.99
			2	150	0.26	1.99	1.99
			1	150	0.79	1.99	1.99

Test series D

The results for test series D, in terms of maximum values of stress components at maximum load, are given in Table 8. Equations used for calculation of stresses are indicated in the table. These stress values are based on the assumption of equal widths of the laminations of the longitudinal and transversal layers according to $b_0 = b_{90} = 150$ mm and of constant ratio $t_{0,k}/n_{CA,k}$ for all longitudinal layers. A nominal beam height $h = 600$ mm and an effective beam height $h_{ef} = 300$ mm are further assumed. For calculation of stress components $\sigma_{t,0,n}$ and $\tau_{yz,n}$ in Table 8 is the width of the first transversal laminations next to the notch assumed to be equal to the full lamination width, i.e. $b_{90} = 150$ mm. The stress components corresponding to the the assumed dominating mode of failure are indicated by being underlined.

Graphs of applied load vs. global beam deflection are shown in Figure 28 for the individual tests and photos from the tests are shown in Figure 29.

For test D1, sounds of wood cracking were noted from a load level of about 250 kN although no significant cracks could be noted. As can be seen in Figure 28, the stiffness decreases at a load of about 300 kN. At a load of about 335 kN, sliding between longitudinal and transversal laminations at the notch was observed. Further sliding over the crossing areas was observed up to, and after, the maximum load was reached. For test D2, a crack in one of the transversal lamination at the notch appeared at a load of 270 kN. A gradual decrease in stiffness can be seen in Figure 28 for load levels of 270-300 kN. At a load of 320 kN, sliding between longitudinal and transversal laminations at the notch was observed. At the maximum load, parallel to grain cracks appeared in both longitudinal and transversal laminations in the reduced cross section above the notch. Sounds of wood cracking without any visible damage was observed at a total applied load of about 300 kN also for test D3. At the maximum load, sliding between one of the external longitudinal laminations and the transversal lamination was observed. For test D4, a small crack was noted in one of the transversal laminations at the notch at a load of 250 kN and sliding between longitudinal and transversal laminations at a load of 290 kN. At maximum load, cracks around knots in one of the external longitudinal lamination located about 200 mm from the notch corner appeared.

Table 8: Failure load (maximum load) and corresponding stress values for test series D.

	F_{max}	σ_x	$\sigma_{x,n}$	$\sigma_{t,0,n}$	$\tau_{xy,gross,n}$	$\tau_{xy,net,n}$	$\tau_{yz,n}$	$\tau_{tor,n}$
	(4)	(55)	(57)	(58)	(59)	(60)	(61)	
	[kN]	[MPa]	[MPa]	[MPa]	[MPa]	[MPa]	[MPa]	[MPa]
D1	350.9	29.2	19.5	38.0	5.48	20.2	<u>0.63</u>	<u>2.52</u>
D2	349.3	29.1	19.4	37.8	5.46	20.1	<u>0.63</u>	<u>2.51</u>
D3	361.6	30.1	20.1	39.2	5.65	20.8	<u>0.65</u>	<u>2.60</u>
D4	345.5	28.8	19.2	37.4	5.40	19.9	<u>0.62</u>	<u>2.48</u>
mean	351.8	29.3	19.5	38.1	5.50	20.2	0.64	2.53

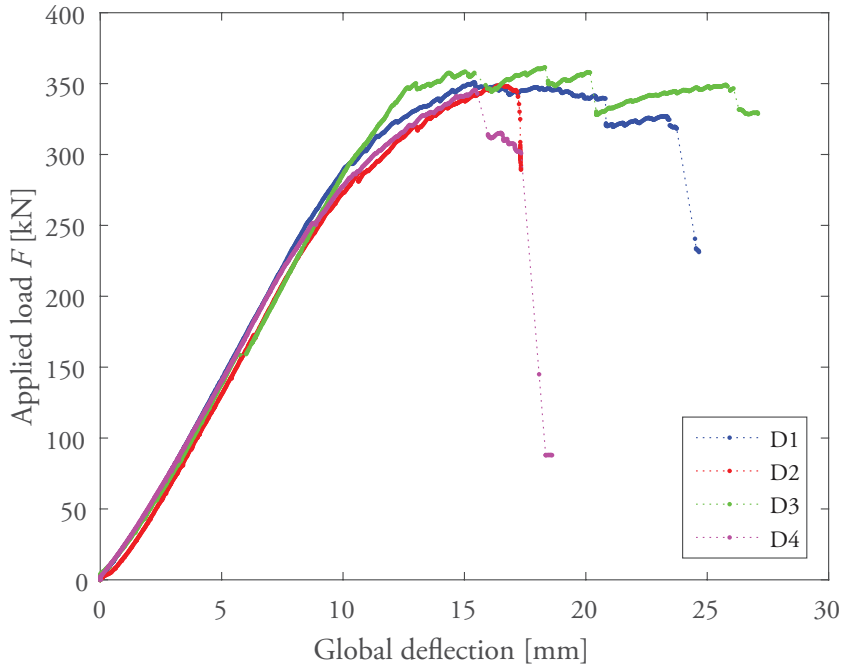


Figure 28: Applied load F vs. global deflection for test series D.



Figure 29: D1 (top left), D2 (top right), D3 (bottom left) and D4 (bottom right).

Test series E

The results for test series E, in terms of maximum values of stress components at maximum load, are given in Table 9. Equations used for calculation of stresses are indicated in the table. These stress values are based on the assumption of equal widths of the laminations of the longitudinal and transversal layers according to $b_0 = b_{90} = 150$ mm and of constant ratio $t_{0,k}/n_{CA,k}$ for all longitudinal layers. A nominal beam height $h = 600$ mm is further assumed. The stress components corresponding to the the assumed dominating mode of failure are indicated by being underlined.

Graphs of applied load vs. global beam deflection are shown in Figure 30 for the individual tests, with beam deflection being measured at the bottom side of the beam at beam mid-span as illustrated in Figure 8. Photos from the tests are shown in Figure 31.

Results in terms of parallel to beam axis shear stress τ_{xz} and torsional shear stress τ_{tor} are also given in Table 10, with stress values based on the actual geometry of the specimens in terms of longitudinal and transversal lamination widths b_0 and b_{90} and ratio $t_{0,k}/n_{CA,k}$ according to Figure 6. An additional (fictitious) reference beam geometry, E-ref, is also included with stress values based on the mean value of the failure load for the four actual tests. The reference geometry is based on assumed lamination widths as $b_0 = b_{90} = 150$ mm. The ratio $t_{0,k}/n_{CA,k}$ is however according to the actual specimens.

For all four tests in test series E, the load bearing capacity in terms of maximum applied load is related to bending failure and cracking due to a combination of bending and tension in the lower-most longitudinal laminations. Before reaching maximum loads, gradual decrease in stiffness can however be noted from the load vs. deflection graphs in Figure 30. For test E2 and especially E4, the beam deflection could be significantly increased after reaching maximum load without loosing more than about 10-15 % of the load bearing capacity. During this loading phase, significant sliding between the adjacent longitudinal laminations was observed. At the final/ultimate failure, cracking and failure of the longitudinal laminations occurred as corresponding to almost pure bending of the individual longitudinal laminations.

Table 9: Failure load (maximum load) and corresponding stress values for test series E.

	F_{max}	σ_x	$\tau_{xy,gross}$	$\tau_{xy,0}$	$\tau_{xy,90}$	τ_{xz}	τ_{yz}	τ_{tor}
		(4)	(12)	(13)	(14)	(19)	(23)	(29)
	[kN]	[MPa]	[MPa]	[MPa]	[MPa]	[MPa]	[MPa]	[MPa]
E1	491.3	<u>35.8</u>	3.84	5.12	15.4	0.77	0.44	1.92
E2	519.5	<u>37.9</u>	4.06	5.41	16.2	0.81	0.47	2.03
E3	513.0	<u>37.4</u>	4.01	5.34	16.0	0.80	0.46	2.00
E4	476.3	<u>34.7</u>	3.72	4.96	14.9	0.74	0.43	1.86
mean	500.0	36.5	3.91	5.21	15.6	0.78	0.45	1.95

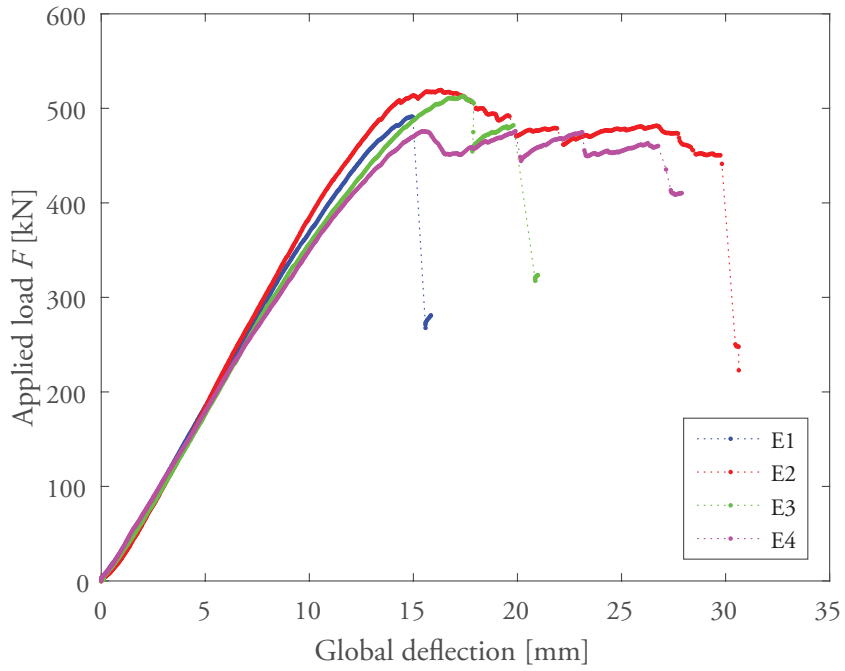


Figure 30: Applied load F vs. global deflection for test series E.



Figure 31: E1 (top left), E2 (top right), E3 (bottom left) and E4 (bottom right).

Table 10: Shear stresses τ_{xz} and τ_{tor} based on actual specimen geometries, test series E.

Specimen	V_{max}	b_{90}	i	$b_{0,i}$	$\tau_{xz,i,1}$	$\tau_{tor,i,1}$	$\tau_{tor,i,1}$
	[kN]	[mm]	[-]	[mm]	Eq. (17) [MPa]	Eq. (32) [MPa]	Eq. (39) [MPa]
E1	245.6	146	5	5	1.35	2.33	5.59
			4	172	0.95	2.74	2.54
			3	172	0.17	2.74	2.54
			2	172	0.61	2.74	2.54
			1	80	1.18	2.33	4.23
E2	259.7	146	5	52	1.31	2.49	5.20
			4	172	0.77	2.93	2.67
			3	172	0.04	2.93	2.67
			2	172	0.86	2.93	2.67
			1	35	1.35	2.49	5.56
E3	256.5	146	4	82	1.24	2.43	4.38
			3	172	0.63	2.86	2.66
			2	172	0.20	2.86	2.66
			1	172	1.02	2.86	2.66
E4	238.2	146	4	135	1.01	2.36	2.77
			3	172	0.35	2.79	2.45
			2	172	0.39	2.79	2.45
			1	125	1.04	2.36	2.98
<i>E-ref</i>	250.0	150	4	150	1.04	2.60	2.60
			3	150	0.35	2.60	2.60
			2	150	0.35	2.60	2.60
			1	150	1.04	2.60	2.60

4.2 Shear stiffness

The shear stiffness of the beams was evaluated considering test series E, prismatic beams loaded in 4-point-bending. A test arrangement and measurement procedure according to the shear field test method presented in the European standard EN 408 [4] was used, see also [1]. Restrictions specified in EN 408 regarding the beam length, distance between load introduction points and distances between load introduction points and supports were however not entirely complied with, see Figures 3 and 8. The shear deformation was measured at a position centrally placed between the support and the closest load introduction point, considering the beam length direction. A total of four deformation measurement devices (potentiometers) were used, two on each side of the beam. The two potentiometers were on each side placed cross-wise at an angle of 90° to each other and at an angle of 45° to the beam axis, see Figures 8 and 32. The arrangement of deformation measurement devices used in the shear field test method is in EN 408 stated as being particularly useful for laminated members such as glued laminated timber.

The effective shear modulus G_{ef} , i.e. the shear modulus considering the beam as homogeneous and of width t_{gross} , is defined as

$$G_{ef} = \frac{\tau_{mean}}{\gamma_{mean}} \quad (71)$$

where τ_{mean} is a mean shear stress and γ_{mean} is the shear strain measured by the two pairs of cross-wise placed potentiometers, see Figures 32 and 33. The shear stress $\tau(y)$ is assumed to have a parabolic distribution over the entire beam height and τ_{mean} is defined as the mean shear stress over the length L in the beam height direction, within which the shear deformations are measured, according to

$$\tau_{mean} = \frac{1}{L} \int_{-L/2}^{L/2} \tau(y) dy = \frac{V}{t_{gross} h} \left(\frac{3}{2} - \frac{h_0^2}{4h^2} \right) \quad (72)$$

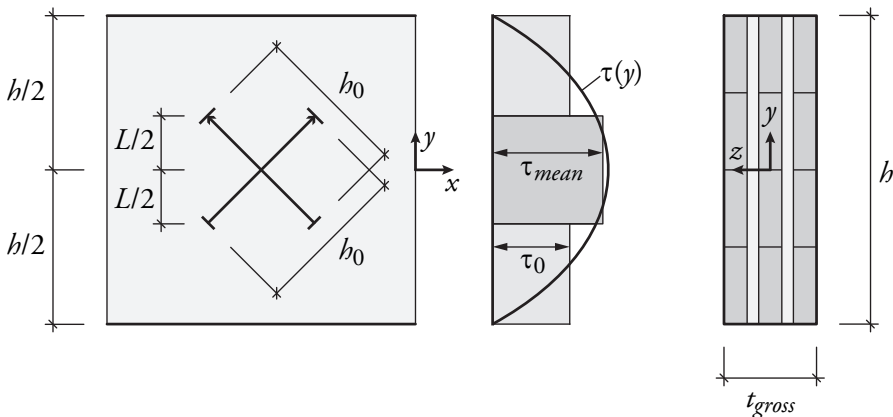


Figure 32: Shear field test method.

The mean shear stress τ_{mean} can be expressed as

$$\tau_{mean} = \tau_0 \alpha \quad (73)$$

with

$$\tau_0 = \frac{V}{t_{gross} h} \quad \text{and} \quad \alpha = \frac{3}{2} - \frac{h_0^2}{4h^2} \quad (74)$$

where τ_0 is the mean shear stress over the entire gross cross section and α is a correction factor, also given to EN 408. The shear strain γ_{mean} is defined according to

$$\gamma_{mean} = \frac{dL}{L} = \frac{\sqrt{2}u}{L} = \frac{2u}{h_0} \quad (75)$$

where u refer to the mean value of the absolute deformations along both diagonals (the *tension* and the *compression* diagonal) on both faces of the beam (the *front* and the *back* face) according to

$$u = \frac{1}{2} (|u_t| + |u_c|) \quad (76)$$

where u_t and u_c refer to the mean value of the readings of the devices along the tension diagonals ($u_{t,f}$ and $u_{t,b}$) and along the compression diagonals ($u_{c,f}$ and $u_{c,b}$) according to

$$u_t = \frac{1}{2} (u_{t,f} + u_{t,b}) \quad \text{and} \quad u_c = \frac{1}{2} (u_{c,f} + u_{c,b}) \quad (77)$$

where the deformation is defined as positive for elongation (tension) and negative for compression.

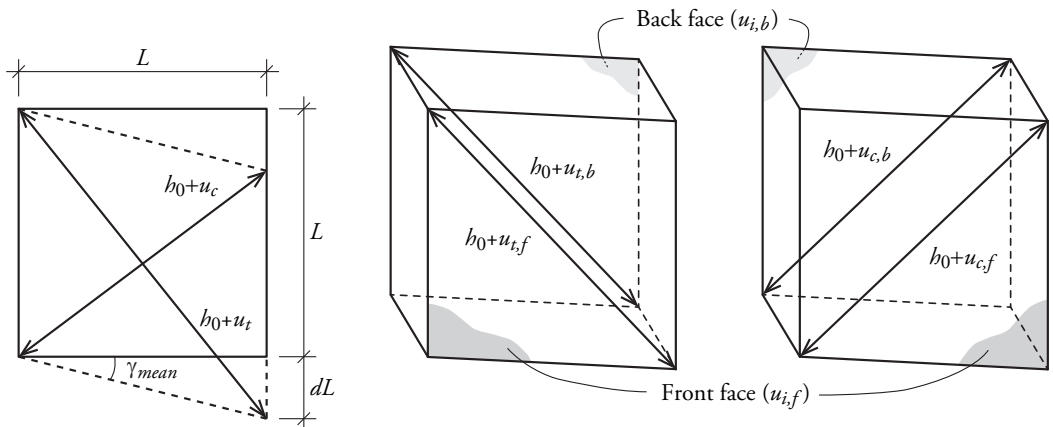


Figure 33: Deformation of tension and compression diagonals on front and back face.

The shear modulus is calculated based on a regression analysis considering only the measurements in the interval $0.1F_{max} < F < 0.4F_{max}$. For all data points within this interval, a linear regression analysis is performed using MATLAB [12] and its built in function `regression` giving a relationship of the form

$$\bar{V} = \bar{u}p + q \quad (78)$$

where p is the slope, q is the intercept and where \bar{V} represent the shear force and \bar{u} represent the mean deformation along the diagonals according to Equation (76). The regression analysis is for each individual tests performed considering data points in the interval $0.1F_{max} < F < 0.4F_{max}$ based on the value of F_{max} for the individual test and not based on the mean value of F_{max} for all four tests of the test series. The effective shear modulus is determined according to

$$G_{ef} = \alpha \frac{h_0}{t_{gross}h} \frac{1}{2} \frac{\Delta\bar{V}}{\Delta\bar{u}} = \alpha \frac{h_0}{t_{gross}h} \frac{1}{2} p \quad (79)$$

where

α	is the correction factor according to Equation (74)
h_0	is the the length over which the deformations $u_{i,j}$ are measured
t_{gross}	is the beam gross cross section width
h	is the beam height
$p = \Delta\bar{V}/\Delta\bar{u}$	is the slope of regression line according to Equation (78)

Results of the measurements and regression analyses are presented in Table 11. The calculations are based on the beam heights h and measurement lengths h_0 as stated in the table. It should be noted that for test E2, the four measurement points on each side of the beam were all placed within a single longitudinal laminations while measurements for the other tests were performed over an area including two different longitudinal laminations.

Table 11: Results of measurements and regression analysis relating to effective shear modulus.

	F_{max} [kN]	h [mm]	h_0 [mm]	α [-]	p [kN/mm]	q [kN]	r [-]	G_{ef} [MPa]
Test E1	491.3	601	240	1.460	306.8	2.872	1.000	559.0
Test E2*	519.5	603	200	1.473	515.6	3.682	0.999	786.9
Test E3	513.0	598	240	1.460	302.7	4.591	1.000	554.2
Test E4	476.3	604	240	1.461	302.6	3.334	1.000	548.7
mean								612.2
std								116.5
cov								19 %

* deformation measurements within a single longitudinal lamination



Figure 34: Placement of potentiometers for E2 (left) and E3 (right) in relation to placement of longitudinal laminations.

4.3 Bending stiffness

The bending stiffness of the beams was evaluated considering test series C, prismatic beams loaded in 4-point-bending. The evaluation included both the local modulus of elasticity in bending $E_{m,l}$ and the global modulus of elasticity in bending $E_{m,g}$ and was carried out according to the directions given in the European standard EN 408 [4]. The restriction specified in EN 408 regarding the beam length, distance between load introduction points, distances between load introduction points and supports and the measurement length over which the local beam deflection is measured were not entirely complied with, see Figures 3 and 8.

The moduli of elasticity in bending are determined based on a regression analysis considering only the measurements in the interval $0.1F_{max} < F < 0.4F_{max}$. For all data points within this interval, a linear regression analysis is performed using MATLAB [12] and its build in function `regression` giving a relationship of the form

$$\bar{F} = \bar{w}_i p + q \quad (80)$$

where p is the slope, q is the intercept and where \bar{F} represent the total applied load and \bar{w}_i represent the local ($i = l$) and global ($i = g$) deflections respectively when considering local and global modulus of elasticity in bending. The regression analysis is for each individual tests performed considering data points in the interval $0.1F_{max} < F < 0.4F_{max}$ based on the value of F_{max} for the individual test and not based on the mean value of F_{max} for all four tests of the test series.

Local modulus of elasticity in bending

The local modulus of elasticity in bending is calculated according to

$$E_{m,l} = \frac{al_1^2}{16I_{net}} \frac{\Delta\bar{F}}{\Delta\bar{w}_l} = \frac{al_1^2}{16I_{net}} p \quad (81)$$

where

$a = 1500$ mm	is the distance between the support and the load introduction point
$l_1 = 1450$ mm	is the length over which the local deflection is measured
$p = \Delta\bar{F} / \Delta\bar{w}_l$	is the slope of regression line according to Equation (80)
I_{net}	is the second moment of inertia, considering only longitudinal boards

Results of the measurements and regression analyses relating to the local modulus of elasticity in bending are presented in Table 12. The measured cross section heights h of the individual beams as given in Figure 6 and presented in the table below are used for calculation of the second moment of inertia I_{net} .

Table 12: Local modulus of elasticity in bending.

	F_{max} [kN]	h [mm]	p [kN/mm]	q [kN]	r [-]	$E_{m,l}$ [MPa]
Test C1	413.2	600	174.9	25.73	0.998	15962
Test C2	363.2	601	188.2	20.33	0.999	17091
Test C3	335.6	600	150.0	24.24	0.996	13692
Test C4	412.9	605	198.0	20.24	1.000	17627
mean						16093
std						1745
cov						11 %

Global modulus of elasticity in bending

The global modulus of elasticity in bending is calculated according to

$$E_{m,g} = \frac{1}{24} \frac{3al^2 - 4a^3}{I_{net} \left(2 \frac{\Delta \bar{w}_g}{\Delta \bar{F}} - \frac{6a}{5G_{ef}t_{gross}h} \right)} = \frac{1}{24} \frac{3al^2 - 4a^3}{I_{net} \left(2 \frac{1}{p} - \frac{6a}{5G_{ef}t_{gross}h} \right)} \quad (82)$$

where

$a = 1500 \text{ mm}$	is the distance between the support and the load introduction point
$l = 4800 \text{ mm}$	is the span length
$p = \Delta \bar{F} / \Delta \bar{w}_g$	is the slope of regression line according to Equation (80)
I_{net}	is the second moment of inertia, considering only longitudinal boards
G_{ef}	is the effective shear modulus
t_{gross}	is the beam gross cross section width
h	is the beam height

Results of the measurements and regression analyses relating to the global modulus of elasticity in bending are presented in Table 13. The measured cross section heights h of the individual beams as given in Figure 6 and presented in the table below are used for calculation of the second moment of inertia I_{net} . A value of the effective shear modulus $G_{ef} = 550 \text{ MPa}$ is further used. This value approximately represents the mean effective shear modulus found from the measurements on test series E (see Table 11), considering only the three specimens where the shear deformation measurements were performed over a part of the beam including two separate longitudinal laminations.

Table 13: Global modulus of elasticity in bending.

	F_{max} [kN]	h [mm]	p [kN/mm]	q [kN]	r [-]	$E_{m,g}$ [MPa]
Test C1	413.2	600	11.62	1.772	1.000	12609
Test C2	363.2	601	12.86	2.196	1.000	14246
Test C3	335.6	600	11.73	3.453	1.000	12753
Test C4	412.9	605	12.52	-0.207	1.000	13471
mean						13270
std						752
cov						5.7 %

5 CONCLUDING REMARKS

This report comprise mainly a presentation of experimental investigations of in-plane loaded cross laminated timber (CLT) beams, including prismatic beams and beams with a hole or a notch. A review of models for calculation of stresses for such elements is also included, in order to facilitate further evaluation of the test results. Some general comments on the test results relating to beam strength and stiffness are given below. Some comments relating to the reviewed models for stress analysis are also given below.

Although the five different test series comprised four nominally equal tests as regards beam geometry in terms of beam height, hole/notch dimension and widths of longitudinal and transversal layers, the individual tests are not nominally equal in the sense that the position and cross section dimensions of some of the individual laminations were different between the beams.

In addition to the results presented in Section 4, measurements using Digital Image Correlation was also performed for three of the tests (A3, B2 and E4). Results from these measurements are not included in this report but will be included in future publications. Measurements of local deformation at supports and at hole and notch corners were also performed, although the results are not presented here.

5.1 Remarks on beam strength

The scatter in beam strength in terms of maximum applied load is overall very low, with a coefficient of variation of 4 % or less for test series A, B, D and E while test series C had a coefficient of variation of 10 %. Due to the complex composition of the elements, with 5-layers of cross-wise bonded laminations in longitudinal and transversal directions, there are more possible modes of failure compared to conventional glulam or timber beam elements. Characterization of beam failure modes, e.g. as bending failure or shear mode III failure, as given in Section 4 and referred to below are based on observations during testing and analysis of the load vs. deflection/deformation response. Assessment of damage initiation and progression and eventually decisive failure mode is difficult since damage initiation appear to often have been in laminations or in crossing areas between lamination which are located inside the beam.

Test series A

For test series A, beams with a hole placed in a position of combined shear force and bending moment loading, two beams failed in bending at the hole and the remaining two beams failed in bending at beam mid-span. Based on the analytical model (see Section 3) for calculation of stresses and assumed mean values of corresponding material strength values, the beams were expected to fail in either bending at the hole or shear related failure at the hole.

Test series B

For test series B, beams with a hole placed with its center in a position of zero bending moment and hence in pure shear, all four beams appear to have failed by reaching the load bearing capacity with respect to shearing in the bonded crossing areas between the longitudinal and transversal laminations (shear mode III) at the two hole corners exposed to tensile stress perpendicular to the beam axis. Based on the analytical model (see Section 3) for calculation of stresses and assumed mean values of corresponding material strength values, this mode of failure was expected to this test series. The experimentally found beam strength is however greater than expected, compared to model predictions.

Test series C

For test series C, prismatic beams loaded in 4-point-bending, all four beams failed in bending. This mode of failure was expected for this test series, although the experimentally found beam strength was slightly greater than expected. The bending failures were all initiated at knots or finger joints in the lower-most longitudinal laminations.

Test series D

For test series D, beams with a notch at the support, the load bearing capacity appears to have been limited by the capacity with respect to shearing in the crossing areas between longitudinal and transversal laminations (shear mode III). The failure behavior is however fairly complex with a gradual decrease in stiffness before reaching maximum load and for some beams a significant load bearing capacity also at increasing imposed beam deflection after reaching the maximum load. The width of the first transversal lamination appear to have little influence on the load bearing capacity in terms of maximum applied load, since the coefficient of variation for the test series is only 2 % while the width of the first transversal lamination is 40, 63, 65 and 146 mm for the four specimens, respectively.

Test series E

For test series D, prismatic beams loaded in 4-point-bending, the final failure of all four beams is characterized as bending failure. The test setup used for test series E was designed in order to induce shear related failures. Although the final failure of all beams seem to relate to cracking in the longitudinal laminations due to bending, this failure may have been preceded by at least partial failure in the crossing areas between longitudinal and transversal laminations.

5.2 Remarks on beam stiffness

The mean effective shear stiffness, as calculated based on the results of test series E and according to the shear field test method in EN408 [4], was found to be $G_{ef} = 612$ MPa. The method used for measurement of shear straining appear however to be sensitive to the placement of the measurement points in relation to the placement of the individual longitudinal laminations and whether the measurements are done within a single lamination or done between two or more adjacent laminations. Considering only the three test series where measurements of shear deformations were carried out over two different longitudinal laminations, and hence including slip between adjacent laminations, the mean effective shear stiffness was found to be about 550 MPa. This latter result agrees rather well with guidelines for approximate values of in-plane shear stiffness of CLT which in literature often is stated as being approximately $0.75G_{0,mean}$, see e.g. [13].

The local and global modulus of elasticity in bending were determined as $E_{ml} = 16093$ MPa and $E_{mg} = 13270$ MPa, respectively, based an evaluation method according to EN 408 [4] of the local and global measured beam deflection of test series C. It should however be noted that the recommendations regarding beam geometry in terms of e.g. beam height to span ratio h/L according to the test standard was not fulfilled.

5.3 Remarks on analytical beam models

Models for stress analysis and models for calculation of beam strength and stiffness for in-plane loading of CLT elements, e.g. as presented in [8], [9] and [10], are reviewed in Section 3. These models are in general based on conventional beam theory considerations with additional assumptions and simplifications to account for the orthogonally layered composition. In addition to the models found in literature and reviewed here, a new and more general derivation for the torsional moment and the torsional shear stresses in the crossing areas between longitudinal and transversal laminations is presented in Section 3.2.3.

The parallel to beam axis shear stress τ_{xz} and the torsional shear stress τ_{tor} are according to the presented models to a significant extent influenced by the lamination widths b_0 and b_{90} of the longitudinal lamination and the transversal lamination, respectively, which are bonded at the considered crossing area. In practical design situations, the engineer will in general not have knowledge about the exact width and location of the individual laminations and hence need to use an estimate based on available information.

REFERENCES

- [1] Brandner R, Gehri E et al: Determination of modulus of shear and elasticity of glued laminated timber and related examinations. In: Proceedings of the International Council for Research and Innovation in Building and Construction, CIB-W18, Meeting 40, Savonlinna, Finland, Paper 40-12-2, 2007.
- [2] DIN EN 1995-1-1/NA:2013-08: German National Annex to Eurocode 5, 2013.
- [3] European Committee for Standardization (CEN): EN 338:2009, Structural timber – Strength classes. Brussels, Belgium, 2009.
- [4] European Committee for Standardization (CEN): EN 408:2010, Timber Structures – Structural timber and glued laminated timber – Determination of some physical and mechanical properties. Brussels, Belgium, 2010.
- [5] European Committee for Standardization (CEN): EN 14080:2013, Timber structures – Glued laminated timber and glued solid timber – Requirements. Brussels, Belgium, 2013.
- [6] European Committee for Standardization (CEN): EN 16351:2015, Timber Structures – Cross laminated timber – Requirements. Brussels, Belgium, 2015.
- [7] European Technical Assessment ETA-15/0906 from 24.02.2016. Cross Timber Systems – CLT, Solid wood slab elements to be used as structural elements in buildings. Austrian Institute of Construction Engineering, Vienna, Austria, 2016.
- [8] Flaig M: Biegeträger aus Brettspertholz bei Beanspruchung in Platteebene. PhD-thesis, KIT Scientific Publishing, Karlsruhe, Germany, 2013.
- [9] Flaig M, Blass HJ: Shear strength and stiffness of CLT-beams loaded in plane. In: Proceedings of the International Council for Research and Innovation in Building and Construction, CIB-W18, Meeting 46, Vancouver, Canada, Paper 46-12-3, 2013.
- [10] Flaig M: Design of CLT beams with rectangular holes or notches. In: Proceedings of the International Network on Timber Engineering, INTER, Meeting 47, Bath, United Kingdom, Paper 47-12-4, 2014.
- [11] Flaig M: In Plattenebene beanspruchte Biegeträger aus Brettspertholz (CLT-beams loaded in-plane direction). Bautechnik 92:741-749, 2015.
- [12] Matlab version R2015b. The Mathworks, Inc, 2015.
- [13] Wallner-Novak M, Koppelhuber J, Pock K: Brettspertholz Bemessung - Grundlagen für Statik und Konstruktion nach Eurocode. proHolz Austria, Immenstadt, Austria, 2013.